INFORMATION TO USERS

This manuscript has been reproduced from the microfilm master. UMI films the text directly from the original or copy submitted. Thus, some thesis and dissertation copies are in typewriter face, while others may be from any type of computer printer.

The quality of this reproduction is dependent upon the quality of the copy submitted. Broken or indistinct print, colored or poor quality illustrations and photographs, print bleedthrough, substandard margins, and improper alignment can adversely affect reproduction.

In the unlikely event that the author did not send UMI a complete manuscript and there are missing pages, these will be noted. Also, if unauthorized copyright material had to be removed, a note will indicate the deletion.

Oversize materials (e.g., maps, drawings, charts) are reproduced by sectioning the original, beginning at the upper left-hand corner and continuing from left to right in equal sections with small overlaps. Each original is also photographed in one exposure and is included in reduced form at the back of the book.

Photographs included in the original manuscript have been reproduced xerographically in this copy. Higher quality 6" x 9" black and white photographic prints are available for any photographs or illustrations appearing in this copy for an additional charge. Contact UMI directly to order.

U·M·I

University Microfilms International
A Bell & Howell Information Company
300 North Zeeb Road, Ann Arbor, MI 48106-1346 USA
313/761-4700 800/521-0600

Order Number 9503525

Flow past an agricultural shelterbelt: Measurements and model results

Adoum, Alkhalil, Ph.D.

Iowa State University, 1994

U·M·I
300 N. Zeeb Rd.
Ann Arbor, MI 48106

Flow past an agricultural shelterbelt: Measurements and model results

by

Alkhalil Adoum

A Dissertation Submitted to the
Graduate Faculty in Partial Fulfillment of the
Requirements for the Degree of
DOCTOR OF PHILOSOPHY

Department: Agronomy
Major: Agricultural Meteorology

Approved:

Signature was redacted for privacy.

In Charge of Major Work

Signature was redacted for privacy.

For the Major Department

Signature was redacted for privacy.

For the Graduate College

Iowa State University
Ames, Iowa

1994

TABLE OF CONTENTS

LIST OF FIGURES

LIST OF TABLES

I. INTRODUCTION

A. Significance of Shelterbelts in Agricultural Practices

Turbulence affects human activities in many ways. The turbulent momentum, heat, moisture, and other scalar (such as CO_2) fluxes within the surface-layer determine the climate in which agricultural crops flourish or wither. Strong winds and their accompanying gusts have a variety of effects on soil, agricultural crops and other man-made structures. Use of shelterbelts helps in many ways to alleviate the harmful effects of strong winds on crops and has often resulted in crop yield increase.

High winds damage plants both directly and indirectly. Direct wind damage can happen at any stage of crop development. Newly sown seeds can be physically removed either soon after they are seeded at a shallow depth or later as seedlings on occasion of high winds. Winds of more than 100 km h^{-1} caused extensive damage to newly seeded crops in Saskatchewan and Manitoba (Canada) in June of 1985 causing many fields to be reseeded (Kort, 1988). Plants are also susceptible to sandblast injury especially at the emergence stage. Depending on plant type, sandblast damage could range from total mortality, to reduced yield, or to delayed maturity. High winds can also cause lodging, which consists of the flattening of crops. Lodging is known to decrease

yield due to photosynthesis reduction and difficulty of harvest. Fruits and flowers could be hurt by sand scouring or they can be simply ripped off before they reach maturity. The leaves rub and damage each other, some are ripped apart for the same reason that a flag frays in strong wind. In general, the extent of wind damage has always been underestimated (Ronneberg, 1992), because it is usually confused with insect damage, water stress, or other factors.

Wind indirectly causes plants to grow dwarf by diverting their energy into growing stronger roots, stems and lignified cells, instead of devoting this energy to grow stems, leaves, flowers and fruits, which results in reduced size and stunted growth (Ronneberg, 1992). High winds also affect pollination by keeping pollinating insects such as bees away. The effects of wind damage are cumulative over the entire growing season and may lead to decreased yields.

Strong winds affect the soil quality as well. Wind transfers momentum downward, causing a shear stress on the land surface. When this stress exceeds the soil resistance forces, soil particles are detached and transported by the wind. Since the wind eroding force is proportional to the cubic power of windspeed, a 20% reduction in windspeed, which is easily achieved by use of shelterbelts, will cause nearly a 50% reduction in erosion force (Skidmore and Hagen, 1977).

In areas where snow makes up a large percentage of the

annual precipitation, such as the Russian steppes and the Great Plains of the United States and Canada, snow accumulation on the ground determines the soil moisture. Shelterbelts and windbreak force snow to fall and accumulate in predetermined location. In a plain area without protection most of the snow is blown into natural depressions and relatively little is left on the field where it is most needed.

Ronneberg (1992) stated that evidence suggests shelterbelts are most effective in marginal areas, where a little help can have a significant impact on growth. Ajayi et al. (1990) reported that crop yields on the lee side of shelterbelts can increase by as much as 50% in semi-arid areas such as the Sahelian region of Africa. This author observed that crop yields increased by an average of 23% through the use of shelterbelts around fields in the Maggia Valley (Niger). The most severe type of productivity loss is that of desertification, which occurs when the land becomes totally unsuitable for agriculture. The Sahel is an ecologically sensitive area because of the threatening desertification due to excessive depletion of existing woodlands, compounded with recurrent drought events. The fight against desertification in that part of Africa adds another dimension to the importance of windbreaks and shelterbelts in agricultural practices. In the region of Tahoua and More (Niger), dunes

that were threatening homes and sugar cane fields were stabilized by planting trees on top of them. An FAO (U.N. Food and Agriculture Organization) program has saved Mauritania nearly 1,975 acres of farm land and 10 km of Mauritania's main southern highway, by stabilizing more than 1,730 acres of sand dunes that would otherwise encroach on the area (Ajayi et al. 1990).

A study by Guyot and Séguin (1978) of the effect of a shelterbelt network on a small region microclimate in Britany (North-west France) showed an increase in the diurnal temperature amplitude (0.5°-1.5°),and a significant reduction (about 30%) in evaporation measured by a Piche evaporimeter.

Shelterbelts improve crop production by controlling wind damage, preserving soil moisture, preventing soil erosion and desertification (Maki, 1982; Grace, 1988; Lyles, 1988; Skidmore and Hagen, 1977, and Scholten, 1988). They are also used as an effective tool to control the spread of pollutant (Sheih et al., 1978). Despite their usefulness there is reluctance to plant and maintain field shelterbelts in the USA (Miller et al., 1975). This reluctance is due to the long period of time invested before the trees provide effective protection and the loss of land occupied by the shelterbelts. Brandle et al. (1992) concluded that a long-term yield improvement of as little as 6% more than compensates for the cost of establishing a shelterbelt and the loss of output from

acres taken out of production. Hence in this era of environmental awareness, shelterbelts and windbreaks present a good alternative to chemical fertilizers to improve agriculture production. The use of well designed shelterbelts for agricultural purposes is, therefore, a good step toward sustainable agriculture, and could be used to combat desertification as well.

B. General Background

Shelterbelts and windbreaks have long been known to improve growing conditions for sheltered crops. Porous wind barriers have been used as an effective method for microclimate management, control of soil erosion, and for crop yield improvement for centuries. They have been found to induce flow patterns in the lee side that modifies the distribution of heat and moisture in both air and soil, as well as the CO_2 concentration in the air (McNaughton, 1988).

The windspeed reduction in the lee of shelterbelts is the result of momentum extraction from the flow by the obstacle thereby enhancing the turbulent kinetic energy (TKE) of the flow (Fig. 1). McNaughton (1988), in his review, described two distinct microclimatic zones in the lee of shelterbelts and windbreaks. This was based on both wind tunnel measurements (Raine and Stevenson, 1977) and field measurements (Radke, 1976), which suggested that a barrier of

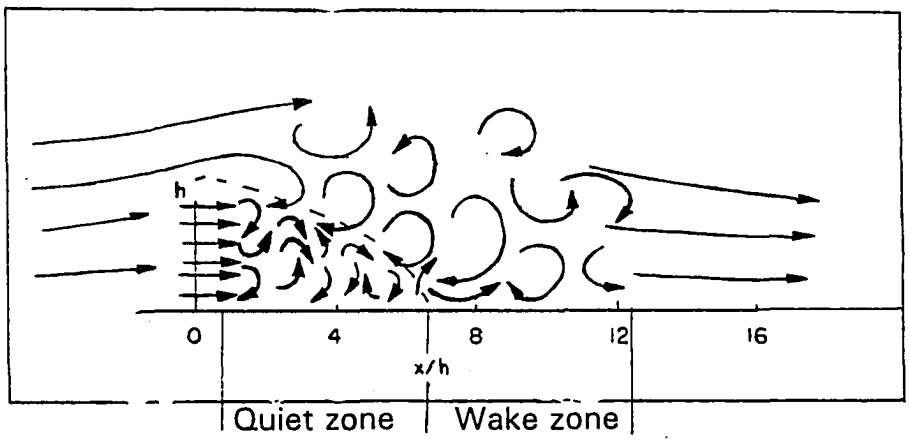

Fig. 1. Schematic representation of turbulence in the wake and in the quiet zone behind a model windbreak. (From McNaughton, 1988).

height H normal to the wind direction, creates a triangular-shaped quiet zone in its lee. This quiet zone extends downwind to about 10H under neutral conditions. Above and beyond the quiet zone is a less-well-defined region of enhanced turbulence called the wake zone.

Turbulent transport of momentum, heat and mass is less efficient in the quiet zone, where both TKE and eddy size are reduced. Near the ground, the equivalent temperature and

humidity are observed to be higher during the day, and the transpiration rate reduced in case of dry air advection. The wake zone, by contrast, has higher TKE values compared to the level upwind. The daytime equivalent temperature and humidity are lower over transpiring crops in the wake zone. The CO_2 concentration is increased and evaporation enhanced with dry air advection. It should be pointed out, however, that microclimate is the sum of many elements, most of which interact, and all can be modified by shelters (McNaughton, 1988).

The capabilities of shelterbelts for increasing yield and for protecting crops and soils from adverse conditions associated with winds, make them valuable tools at the agronomist's disposal. In order to optimize the use of shelterbelts, scientists have concentrated their efforts on understanding the interaction of porous shelters with the flow field as a prerequisite to understanding the resulting microclimatic implications. Several avenues are used by researchers to explore the aerodynamics of shelterbelts and the microclimate in their lee.

Simplifications of the equations of motion often lead to analytical solutions. The resulting models may be physically unrealistic, or somewhat oversimplified, but are often useful. In his review, Plate (1971) used an analytical model that was able to reproduce the shear stress distribution. Counihan et

al. (1974) used an analytical model to show the relationship between the wake and the pressure field close to the obstacle. They acknowledge, however, that the theory failed to adequately describe the distribution of shear stress and turbulence intensity across the wake.

The most reliable information about a physical process is often given by an experimental investigation involving full-scale measurements. Such experiments in most cases are prohibitively expensive. For instance measurement of turbulent flux profiles at several locations around a shelterbelt could be very costly since it requires the use of fast-response sensors. It is also possible to perform experiments on small-scale models (wind tunnels), and extrapolate the resulting information to full-scale using similarity law. The attractive feature of a scale model is that experimental conditions are easier to control. But small-scale models do not always simulate the features of full-scale phenomenon (Patankar, 1980). Another alternative is numerical modeling. Numerical simulations are based on fundamental laws of physics and are mathematical representations that describe physical features of the flow. Numerical models have the advantage of producing results very fast and at a relatively low cost as compared with field experiments, although it is common to overlook the time invested in developing them. Most models require tuning for

slightly different problems, but once they are tuned and tested they have the ability to simulate ideal conditions for studying basic phenomena. In other words numerical models make idealizations extremely easy. Regardless of the method used, the goal of research on shelters is to characterize their effectiveness for reducing windspeed, protecting the soil against erosion, and creating more favorable microclimatic conditions for optimal plant growth in the lee side.

For the sake of comparison, windbreaks and shelterbelts are categorized according to their internal as well as external structure (Bean et al., 1975). Porosity is found to be the major physical parameter that determines effectiveness in reducing windspeed (Hagen and Skidmore, 1971a; Wilson, 1987). The porosity is easily calculated for simple artificial wind barriers (e. g., a fence that has no depth), since it simply represents the optical porosity. It is, however, much more difficult to estimate porosity for three-dimensional, living, aeroelastic barriers such as tree shelterbelts, which are inhomogeneous in all three directions and have a wide range of barrier element rigidities (e. g., trunks, branches, twigs, leaves, needles). The term density (used interchangeably with porosity) is more appropriate as an index of permeability for three-dimensional barriers. No attempt has been made so far to give shelter density a formal

definition but it implicitly represents the ratio of plant element volume to the total volume occupied by the plant including the gaps. An increase in density is, thus a decrease in porosity and vice-versa. Photographic techniques sometimes have been used to estimate porosity for living shelters (Jensen, 1954; Maki and Allen, 1978). Since optical porosity does not adequately describe the three-dimensional spaces through which the air flows, a more dynamically consistent alternative is needed. Wilson (1985) used the leaf area density, whereas Litvina (1987) used a parameter that took into account the three-dimensionality of the plant, with other characteristics used to describe the overall shape or external structure. These include height, species, number of rows, spacing between rows, and spacing between trees.

Many investigators have studied windbreak windspeed reduction and have made different assertions as on how much the windspeed is reduced, or how far downwind the windspeed reduction extends. Van Eimern et al. (1964) came to the conclusion that the wind recovered at a shorter distance in the lee of denser shelters, although the windspeed reduction is higher in the near lee for denser shelters. They explained this by the fact that largest velocity reduction in the near lee resulted in larger shear. As a consequence, more turbulent kinetic energy (TKE) is produced which tended to smooth the gradients and led to more rapid recovery. This

interpretation was accepted until it was challenged by Wilson (1985), who noted that data by Hagen and Skidmore (1971b), and Raine and Stevenson (1977) showed that denser shelters provided more protection at all distances in their lee. He argued that the TKE produced was at small scale and consequently it contributed little to the momentum transport and dissipated rapidly. Heisler and DeWalle (1988) attributed the apparent conflict between recent and older work to a failure to observe similarity requirements in comparing the older field experiments.

Measurements showed the existence of a sharp speedup over fences (Bradley and Mulhearn, 1983; Hagen and Skidmore, 1971b), which created a zone of large velocity shear immediately above the top. This zone, already referred to as the wake zone, widens and follows the streamline as the air moves downwind and acts as a strong TKE source (McNaughton, 1988). The increase of turbulence behind a fence was clearly evidenced by the work of Ogawa and Diosey (1980), and Heisler and Dewalle (1988). Their data showed that spectral peaks shifted from lower frequencies upwind to higher frequency behind the shelter (at 5H downwind), and generally recovered to their lower frequencies further downwind. An analysis in streamline coordinates by Finnigan and Bradley (1983) revealed that the TKE showed an increase of about 50% over the upstream value to at least four fence heights. This feature was also

shown by the data of Perera (1981).

Bradley and Mulhearn (1983) also measured the momentum transfer to the ground with drag plates and found that the fence reduced the stress below 75% of its value in the open out to a downwind distance of 10H. Seginer (1975a) found atmospheric stability to have a systematic and significant effect on the windspeed reduction as well. He indicated that the relative windspeed at any distance from the windbreak could be expressed as an empirical function of the Richardson number under unstable conditions. Bradley and Mulhearn (1983) speculated that wake flow appeared to be particularly sensitive to buoyancy effects and more so to slight stability than to slight instability. Perera (1981) conducted a series of experiments with different porosities and different shapes of openings. He concluded that it was in fact the porosity and not the form of the construction of the fence that determines the structure of the wake flow.

Bilbro and Fryrear (1988) and Grace (1988) have analyzed and generalized recent research results on microclimate and yield to find a basis for making practical recommendations on wind barrier design. An ideal shelterbelt design procedure would use shelterbelt aerodynamics parameters to simulate the complete microclimate, which in turn, would be used to predict yield. In that respect Wilson (1985) generated design aids from the prediction of a second-order closure model. Litvina

(1987) used a one and a half closure model that takes into account the shelter physical properties in the parameterization of the turbulence length scale. She defined a wind-sheltered effectiveness, a soil-sheltered effectiveness, and a deposition (snow or dust) effectiveness; and these were used as design criteria.

Wilson (1985) investigated the patterns of flow through a porous windbreak by making use of several well-known turbulence schemes. Although his results were somewhat satisfactory in the near wake, all simulations failed to predict the sharp speedup over the fence. As a consequence, this deficiency caused a slower recovery rate than observed. In their analysis, Finnigan and Bradley (1983) confirmed that the abrupt increase of TKE at all levels above the fence would be consistent with pressure transport from a region of enhanced production in the decelerated flow immediately upwind. Although they didn't have the data to support their claim, they strongly suggested further investigation.

C. Significance of the Present Research

The discussion so far has shown that many aspects of shelterbelt effects have been to some extent explored. There is, however, some disagreement in the literature about certain issues. The main objective of this study is to investigate

such issues as the extent of shelter protection in relation to shelter density, and the dependence of windspeed reduction on free stream velocity (angle of incidence and speed).

Usually the relative windspeed u/u_0 (where u_0 and u are the windspeeds in the open and in the lee, respectively) is used to compare the wind reducing effect of shelterbelts. This practice ignores the indirect effect of u_0 on u (Eimern et al., 1964). Sometimes the minimum relative windspeed u_m/u_0 (u_m is the minimum windspeed in the lee) is used as an index of shelter density (Heisler and DeWalle, 1988). However, this led the authors to conclusions that contradicted conventional established wisdom. Results from such studies could be misleading because 1) given the coarse resolution that characterizes field experiments u_m is hard, if not impossible to locate; 2) there is evidence that u_0 affects the density of shelterbelts and density is known to have an impact on u_m and its location in the lee (Hagen and Skidmore, 1971b; Raine and Stevenson, 1977). Contradicting reports about the effects of angle of incidence also exist. Sturrock (1969) considered this factor to be insignificant, while Woodruff and Zing (1955), Seginer (1975b), and Mulhearn and Bradley (1977) concluded otherwise. The results by Woodruff and Zing showed that the barrier provided only one half the protection obtained when the wind approached the barrier perpendicularly. The study by Mulhearn and Bradley indicated that the flow

close behind a shelter is significantly affected by the orientation of the shelter relative to the wind direction, and more so for shelters with smaller aspect ratios (height-to-length ratio). Measurements by Seginer (1975b) suggested that the relative windspeed in the lee was strongly dependent on the angle of incidence. Thus, studying the effect of free stream velocity (both speed and direction) on the windspeed reduction, will help shed some light on the aforementioned issues.

The relationship between the extent of protected distance in the lee and the shelter density is subject to controversy. Naegeli (1946), cited in Eimern et al. (1964), suggested that medium-dense shelters provided more protection (e.g. a longer protected zone) downwind than the very dense ones, while Wilson (1985) claimed that denser shelters provided more protection. A review by Heisler and DeWalle (1988) seemed to support Wilson findings. Before we rush into rejecting the old theory, a strong proof is needed that the new one is trustworthy. Heisler and DeWalle compared data from three previous experiments: Caborn (1957), Naegeli (1946) and a combination of Sturrock (1969) and (1972). Although the use of the relative minimum windspeed as a density index was not appropriate, there was qualitative agreement between data from two of the experiments (Caborn, 1957; Naegeli, 1946). These data showed that the length of the protected zone increased

with increasing u_m/u_0 until it reached a maximum at about $u_m/u_0=0.25$, then decreased with further higher values. However, data from the combined field experiments of Sturrock showed a steady decrease of the protected length with increasing u_m/u_0 in Heisler and DeWalle review. A look at the actual Sturrock (1969) work showed that, in more than half of the cases where comparison of the density effect was possible for the same shelterbelt (leafless, half leaf and full leaf), the length of protected distance is shorter for the very dense case (full leaf).

Measurements with artificial barriers in the atmosphere (Hagen and Skidmore, 1971b) or in wind tunnels (Raine and Stevenson, 1977) showed only a slight fall-off of the protected distance for solid fences, far smaller than the fall-off suggested by Naegeli (1946). Wilson's (1985) conclusions were based mainly on his own numerical simulations. Numerical and wind tunnel models offer convenience in both operational cost as well as control of experimental conditions, but the resulting simulations cannot be expected to be similar in every aspect to observations on shelterbelts. The same could be said about full scale artificial barriers that are purely two-dimensional and rigid, where the effects of branches and foliage movement cannot be replicated.

The above evidence suggests that Wilson's claim can be

challenged. Although we don't have an appropriate data set to explore this issue, the modified two-dimensional Litvina model will be used to study it. The Litvina model is appropriate to conduct this type of study because it has a unique feature. The sink term in the momentum and the source/sink term in the TKE equation have in addition to the drag coefficient a shelter density parameter that accounts for the three-dimensionality of shelterbelts.

Experimental data will be used to study the effect of free stream velocity and to test the modified Litvina model. The validated model then will be used to explore the controversial issue about windspeed reduction and the extent of protection downwind and to compute shelter efficiency and study its relationship to shelter density. Sensitivity tests will be performed, and the TKE distribution explored as well.

II. DATA ANALYSIS AND MODEL VALIDATION

A. Source of Data - Site and Instrumentation

The data used in this project consist of vertical profiles of windspeed, temperature, and measurement at one level of wind direction, relative humidity, and the differential pressure across the belt. They were collected during a field experiment that took place from September 21 to September 28, 1993. This experiment was the result of a joint effort between the University of Nebraska, the Rocky Mountain Forest and Range Experiment Station, and Iowa State University. It was the first of a series of field measurement programs scheduled for the next three years at the University of Nebraska Shelterbelt Research Facility. This facility is at an experimental farm operated by the University of Nebraska, located approximately 50 km north of Lincoln near Mead at 41°10′N and 96°40′W (Schmidt and Jairell, 1993).

The belts consist of two rows, which are 3 m apart, of alternating pairs of green ash and white pine planted in 1966. During the measurement period the belts average width and height were estimated at 8 m and 12 m, respectively. There are several shelterbelt arrays on the farm (Fig. 2), of which the southern one was chosen for this experiment. The chosen array consists of two east-west 264-m-long legs that are 132 m apart, linked by a north-south leg at the west end.

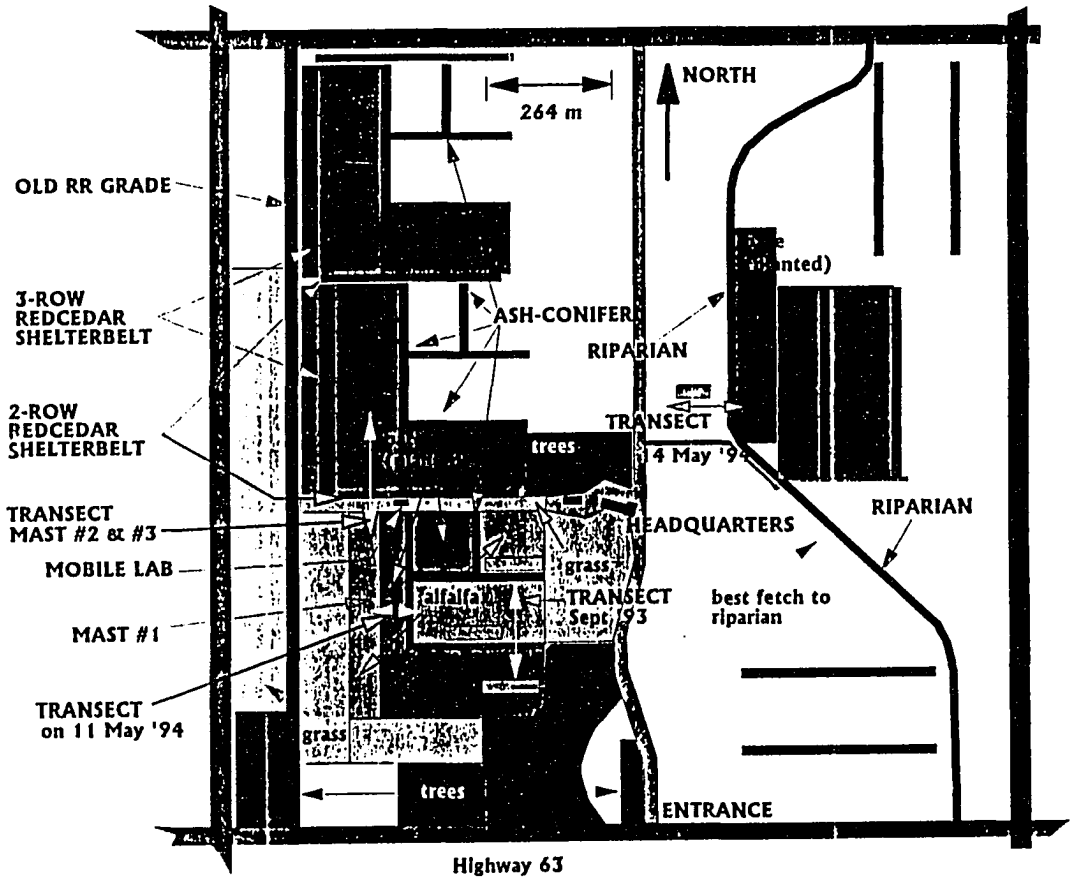

Fig. 2. Shelterbelt arrays at the experimental farm.

The vertical profiles of mean windspeed and temperature were obtained by using three 10-m masts along a transect perpendicular to the east-west legs (Fig. 2). Mast 1 was at 7H, centered in a harvested vegetable plot surrounded by a bean field, south of the southern leg. The other two masts were moved to several locations across the alfalfa plot between the two east-west legs of the array during the experiment.

Each mast includes a free-standing support and arms holding cup anemometers and thermistors up to 10-m height (Fig. 3). The sensor support arms are attached to the mast at right-angle with welding clamps for easy adjustment of sensor heights. Sensors attach by waterproof connectors, with the cup at the end of the arm 60 cm from the mast. The thermistor attaches midway between the anemometer and the mast. Two connectors at the mast end of each support arm connect sensor signals to the mast cable harness. The lowest seven sensor arms are attached to a right-angle piece so that all are moved as a ganged rack. In addition, each mast supports an R.M. Young propeller-vane near the 4-m level. Mast 1 and 3 supported Model 05303 (-AQ) and Mast 2 held Model 05701 (-RE). Mounted on the back of each mast, a Campbell 207 probe in a 12-plate Gill radiation shield measured temperature and relative humidity (RH) at the 1.5-m height. On mast 1, a LI-COR, Inc. pyranometer (LI-200SZ) measured global sun plus sky

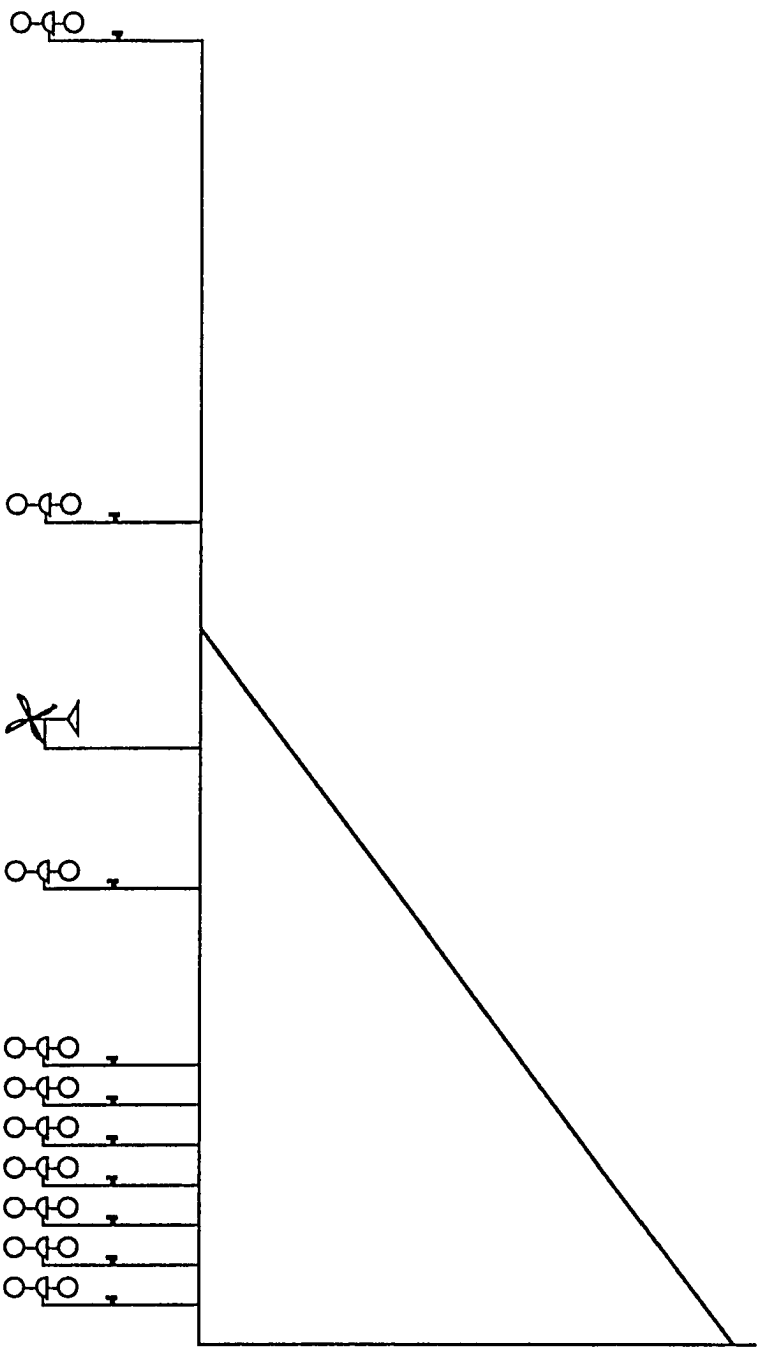

Fig. 3. Observation mast used for the experiment.

radiation near the 1.2-m height. A differential pressure transducer (Setra Systems, Model 264) measured pressure change between the two sides of the shelterbelt at the surface.

The wind profiles were measured by three-cup anemometers (Maximum Inc. Model 40). The cups are canonical in cross-section with 5-cm maximum diameter, and the rotor sweeps through a 19-cm diameter. The cup centerline is 8.4 cm above the top of the support arm. The threshold of the cup is 0.45 m s^{-1}. There is a tendency in cup-anemometers to overspeed resulting partly from its non-linear response to windspeed and partly from sensitivity to the vertical component of the velocity. Propellers do not overspeed, but they operate dependably only when pointing directly into the wind. In other words they are also sensitive to the vertical component of the wind. The Maximum Inc. Model 40 instruments are lightweight cup anemometers with accuracies and constants comparable to propeller-vane anemometers (Kaimal and Finnigan, 1994). Measurements by a cup anemometer were compared to windspeed indicated by an R. M. Young propeller vane (Model 05701), whereby an equation to correct for overspeeding was found.

$$\text{windspeed (m s}^{-1}) = 0.49184 + 0.89434 * \text{cup estimate (m s}^{-1})$$

The first and seventh days of the experiment were the only days where the wind had a southerly component. These cases were extremely important for this study, for when the

flow had a southerly component the mast south of the southern leg of the array measured the upwind (unprotected) flow. This was not the case when the wind had a northerly component, because the upwind masts were protected by the northern leg of the array. These cases were also of capital importance for comparing simulations with observations, since the model used the flow profile in the open (upwind unprotected flow) to simulate profiles in the lee.

B. Relationship between Angle of Incidence and Wind Direction in the Lee

Our interest in studying this relation stems from the fact that two-dimensional shelterbelt models such as the Litvina model always assume the flow to be perpendicular to the shelter. Unfortunately this assumption is not always true. If the flow crosses the shelterbelt without being deflected, then it will be possible to use the profile of the normal component of the wind as a boundary condition for the model. If on the contrary the flow undergoes a significant deflection then it may not be possible to use the wind normal component as a boundary condition.

Wind direction at the three masts and the distance of mast 3 from the shelter for day 264 (mast 3 was moved to 5 locations on that day) are depicted in Fig. 4, and the corresponding windspeed is shown in Fig. 5. We can see that

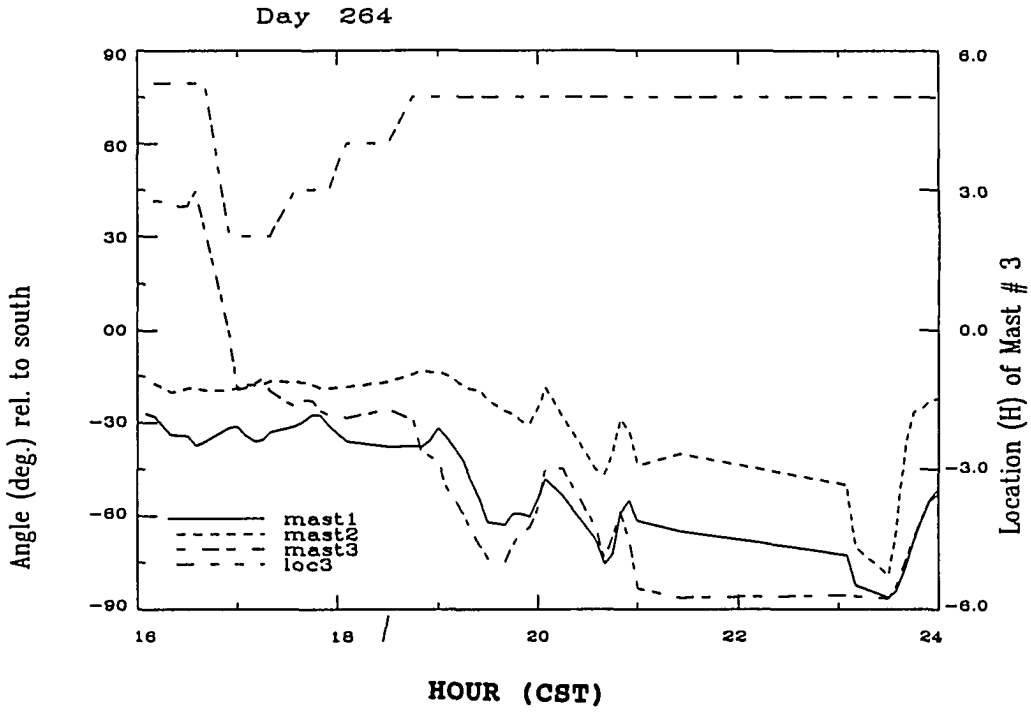

Fig. 4. Wind angle (deg.) with the normal to the belt for all three masts and distance in shelterbelt heights (H) of mast 3 from the shelterbelt.

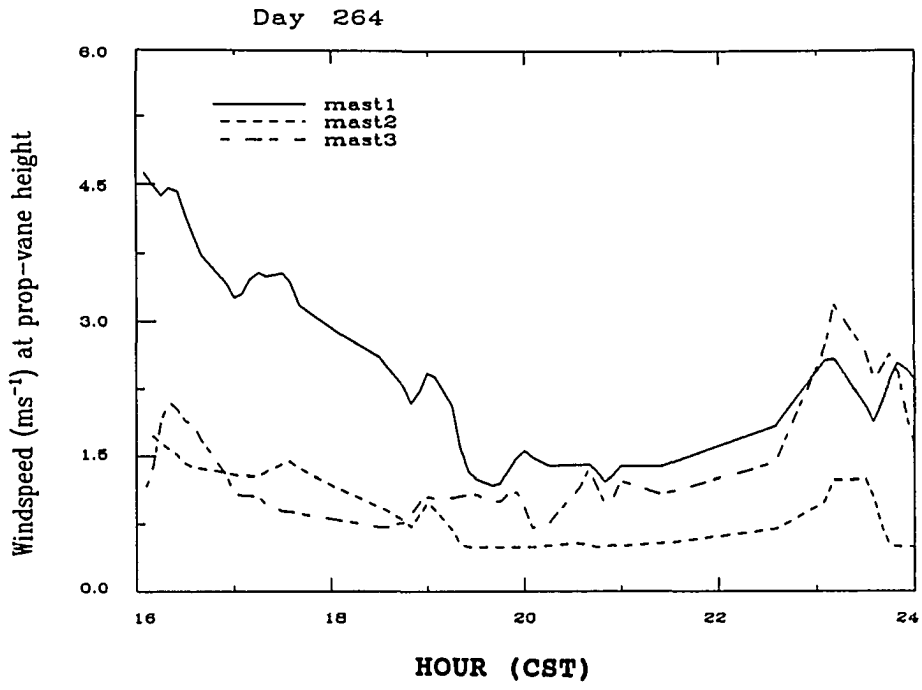

Fig. 5. Windspeed (ms^{-1}) for all three masts.

from the start (16:05 CST) to 16:40 CST (all times given in CST) the wind hits the shelter at about 30° from the normal (this angle will be referred to as the approach angle or incidence angle). In the lee at mast 2 the vane recorded a decrease in the approach angle. Further downwind at 5.3H mast 3 recorded an even larger deflection; that is the flow became northwesterly (40-45°). At 16:50 mast 3 was moved closer to the shelter (2H). As a result, the wind angle at mast 3

became closer to the one at mast 2, but the approach angle stayed slightly smaller until after 17:20 when mast 3 was moved to 3H, 4H, and 5H (Fig. 4) at 17:25, 18:05, and 18:45, respectively. During that period the wind vector-transect angle at mast 3 remained smaller than the one at mast 1, but larger than the one at mast 2 (comparisons are made in absolute value).

Fig. 5 shows a decreasing windspeed with time. After 19:20 the windspeed at mast 2 is below the cup anemometer threshold which is 0.49 m s^{-1} (Schmidt and Jairell, 1993); the speed shown is solely due to the cup anemometer threshold correction. Furthermore the wind shifted to east-south-east, and the approach angle of the wind became larger than 50°. The distance between the transect and the eastern end of the shelterbelt is 5.5H. Let's imagine a straight line parallel to the wind vector and passing by the eastern end of the shelter through the location of mast 3 at 5H makes an angle $\alpha=\tan^{-1}(5.5/5)$ or $\alpha=48°$ with the normal. For angles near or larger than this, mast 3 will be in the middle of the zone under the influence of the tip vortices. Thus, because of the weak winds and their angle with the perpendicular to the shelter, the analysis does not extend to data recorded after 19:20 on day 1 of the experiment (Julian Day 264 corresponding to Sept. 21, 1993).

Mast 2 remained close to the belt throughout the day and

we observed that the angle between the wind vector and the normal to the shelter is always smaller than the one upwind of the shelter. These observations suggest that the shelter tends to orient the wind more normal to the shelter. This deflection is most probably caused by the pressure gradient across the shelterbelt. As illustrated by Schmidt and Jairell (1993) there is a pressure build up in the upwind side and a deficit in the lee, resulting in a pressure gradient across the belt (Fig. 6). The pressure change ΔP across the shelter varied from 0 to 4 Pa for winds with southerly component. The magnitude of pressure drop is about a typical atmospheric

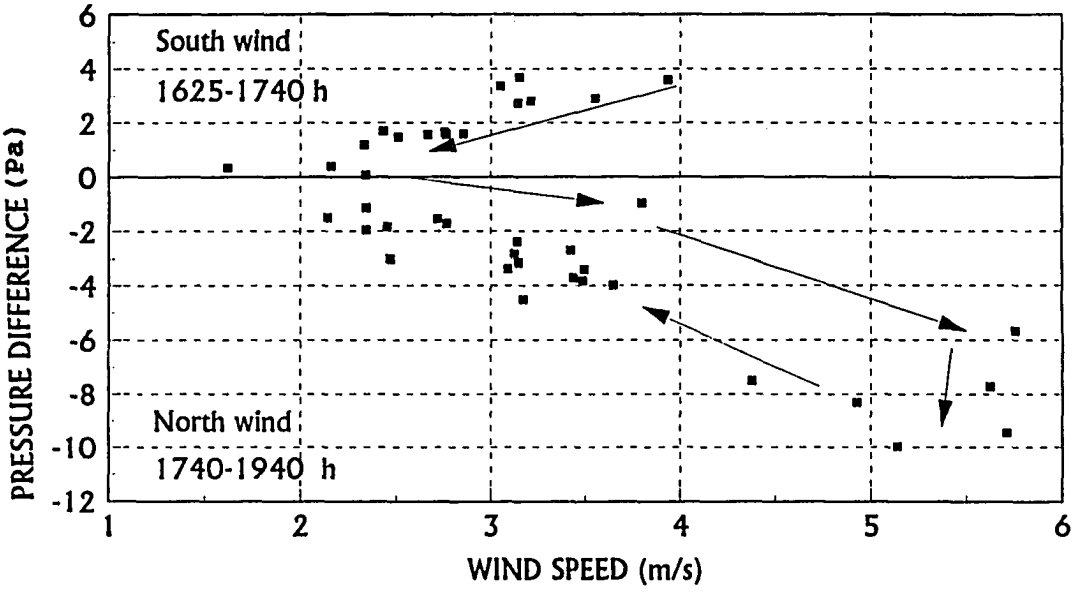

Fig. 6. Pressure difference across the shelterbelt vs wind speed at the top of mast 1. (From Schmidt and Jairell, 1993).

pressure change within a distance of about 1 km (Seginer and Sagi, 1972). In other words the pressure gradient across the shelter is 100 times larger than a typical atmospheric horizontal pressure surface gradient. But of course, we don't observe supersonic jets through the belt pores because of two reasons: 1) generally both frictional and drag forces are proportional to $\nabla^2 u$ (Pedlosky, 1987) and u^2 (Panofsky and Dutton, 1984), respectively. 2) the horizontal distance where strong pressure gradients prevail is extremely short, so the acceleration time is short and the velocity increase small.

The pressure distribution along the transect at the ground is depicted in Fig. 7. It is characterized by an upwind pressure increase that reaches a maximum at about 1H ahead of the shelter. This maximum is followed by a sharp decrease of pressure across the shelterbelt to a minimum about 4H downwind. The pressure then increases slowly toward full recovery.

This pressure distribution affects the balance of forces acting on an air particle as depicted in Fig. 8. For the sake of illustration, we imagine an oblique undisturbed flow with the synoptic-scale isobars forming a small angle with the parallel to the shelterbelt. At point a) far upwind (14H), the balance is between the pressure gradient force ($\mathbf{F}_p$), the Coriolis force ($\mathbf{F}_{co}$), and the friction force ($\mathbf{F}_r$). Further downwind at point b) the shelter pressure-gradient force ($\mathbf{F}_{ps}$)

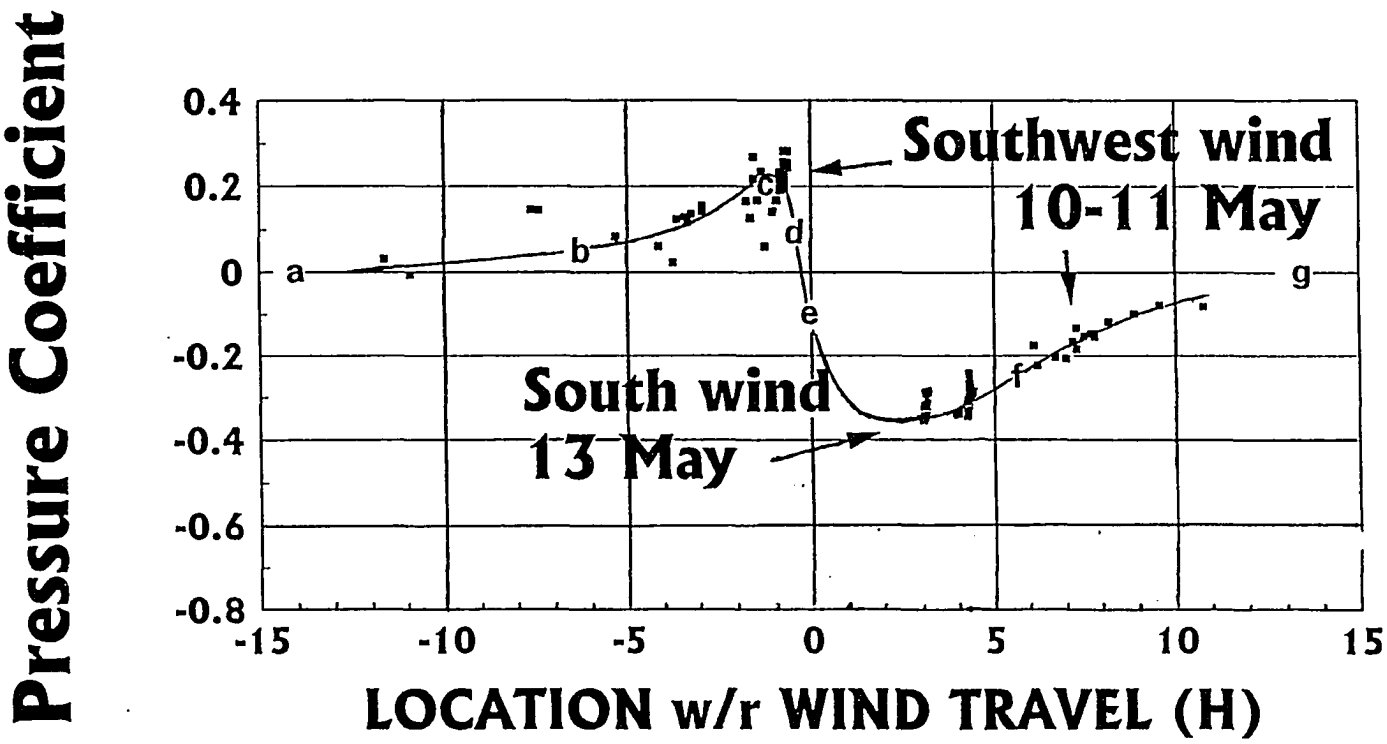

Fig. 7. Static pressure normalized by the dynamic pressure at 10 m level (after Schmidt and Jairell, 1994).

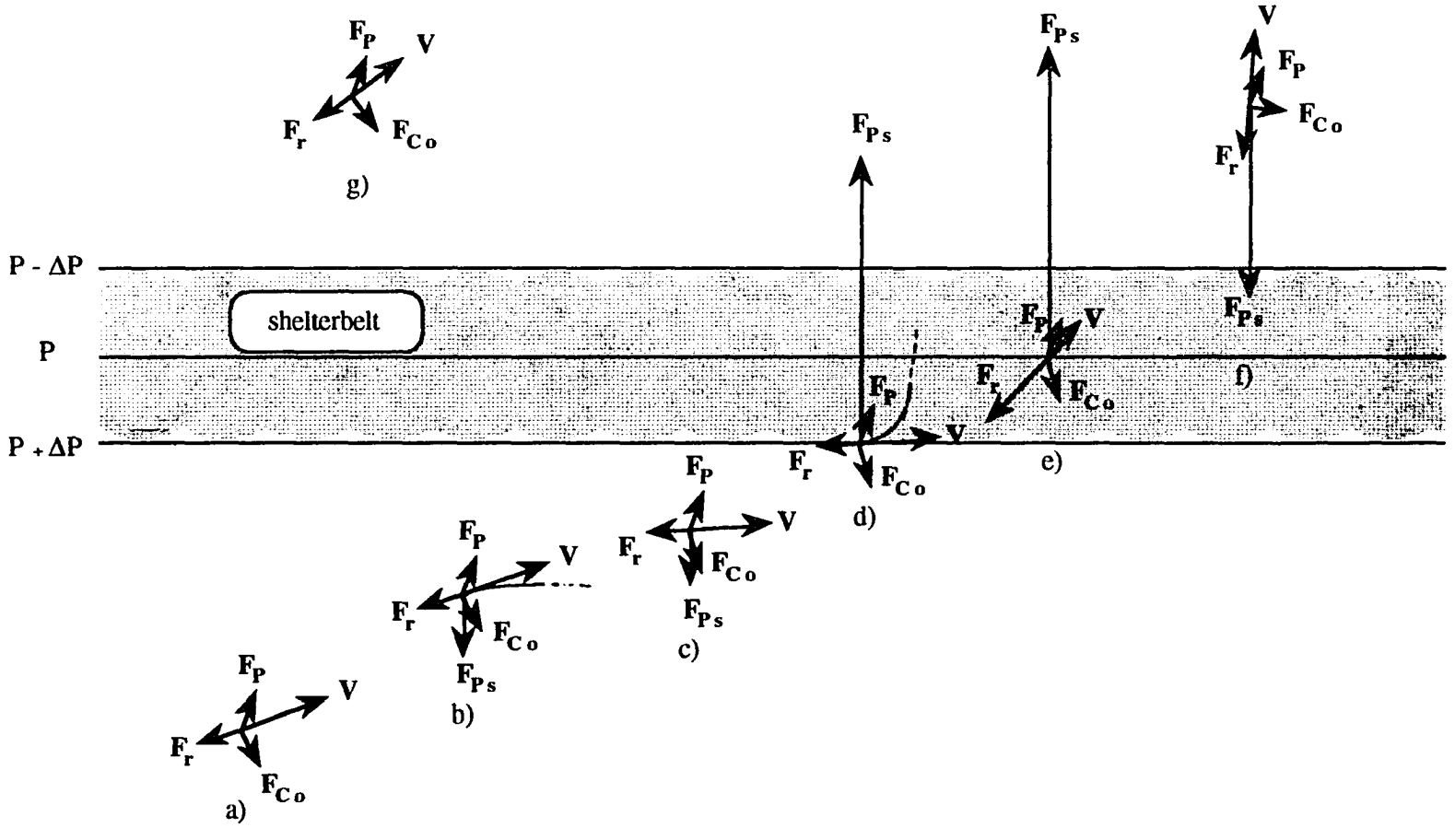

Fig. 8. Schematic representation of the forces acting on an air parcel approaching and passing a porous shelterbelt, where a, b, c, d, e, f, and g, correspond to locations denoted by the same letter as in Fig. 7.

comes into play. This force is perpendicular to the shelter for a uniform shelterbelt. F_{ps}, being larger than the other forces, will have two effects on the flow: a deceleration and a rotation toward a line parallel to the shelter (dotted curve of sketch b Fig. 8). About 1.5H upwind of the shelter (point c) close to the pressure maximum, the shelter pressure-gradient diminishes and so does F_{ps}. Between the extremes F_{ps} becomes very large. Its effect is the same as previously described (deceleration and rotation of the wind vector), except that this time the rotation is toward a perpendicular to the shelter (sketch e, Fig. 8). As the flow starts crossing the shelter, F_r also becomes large because of the shelter drag. Beyond the minimum at point f) F_{ps} reverses again but fades quickly as the flow moves away from the shelter. Further downwind at 13H the recovery process is under way. Note that although F_{co} is normal to the velocity it doesn't play a significant role in the recovery process. It is the turbulent transport that ensures the recovery.

At mast 3 the wind direction, before 16:50, has a westerly component, suggesting that the flow is forced to almost reverse its course. This strong deflection is likely to be the result of the effect of the shelterbelt edge vortices (Mulhearn and Bradley, 1977) at the eastern end.

For day 270 the wind was blowing from the southwest (Fig. 9), and the windspeed at 3.18 m stayed above 3 m s^{-1} until

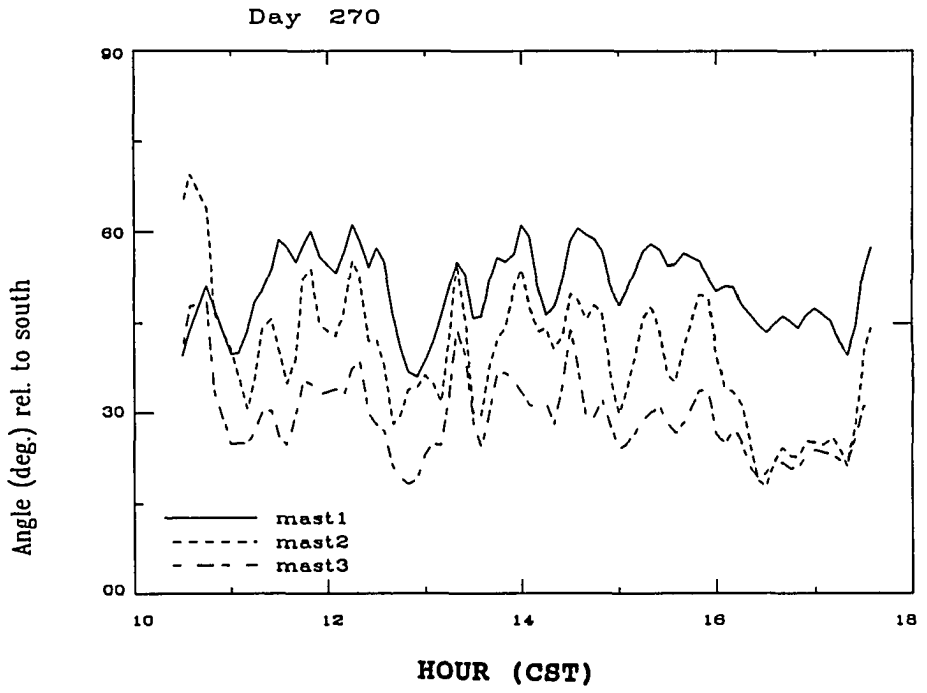

Fig. 9. Wind angle (deg.) from the normal to the shelter for all three masts.

16:00 (Fig. 10). Furthermore mast 3 was kept closer to the shelter at 1H, and mast 2 at 2H. The windspeed at mast 2 is, as expected, slightly higher than at mast 1 (Fig. 10). The wind direction displayed a pattern that is consistent with the previous case (Day 264), when the two masts in the lee were closer. Mast 3, being closer to the shelter, recorded the smallest angle with the perpendicular to the shelter, and

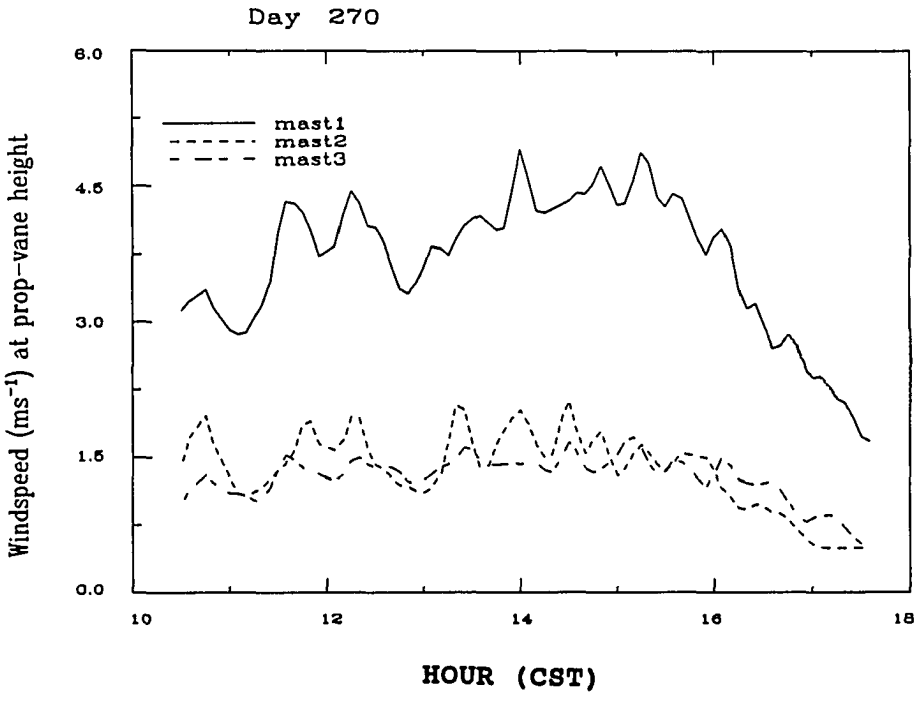

Fig. 10. Windspeed at about the propeller-vane height (3.18 m) for all three masts.

mast 2 recorded a larger angle, suggesting as before that the pressure gradient being perpendicular to the shelter, pulls the flow along the parallel to the transect. This effect gets smaller away from the shelter, where the relative importance of the pressure gradient across the shelter is reduced. On Day 270 both Mast 2 and Mast 3 were close to the shelter at 2H and 1H, respectively. They were, therefore, both under the shelter protected zone and away from the tip vortex influence.

Both wind angle and speed are more sensitive to abrupt changes in the free stream flow at 2H (mast 2) than at 1H (mast 3). As indicated in Fig. 1, the quiet zone is deepest close to the shelter, but becomes shallower downwind, while the wake zone becomes deeper. The wake eddies, being more efficient in transferring momentum, cause the flow further in the lee to respond faster to changes in the undisturbed upwind flow.

C. Influence of the Approach Windspeed and Angle of Incidence

The relationship between the speed of the attack flow and its reduction by shelterbelts as well as the relationship between the angle of incidence and windspeed reduction in the lee were studied by means of regression at three different levels. A preliminary examination showed a strong correlation between the explanatory variables. It was very likely that the strong correlation between the wind direction and its speed would be attributable to the prevailing synoptic situation of the day.

1. Effect of the undisturbed windspeed

Our study revealed that the speed of the approach flow and the reduced windspeed in the lee were positively correlated (Fig. 11). The most often sought quality of a shelterbelt is its ability to extract momentum from the mean

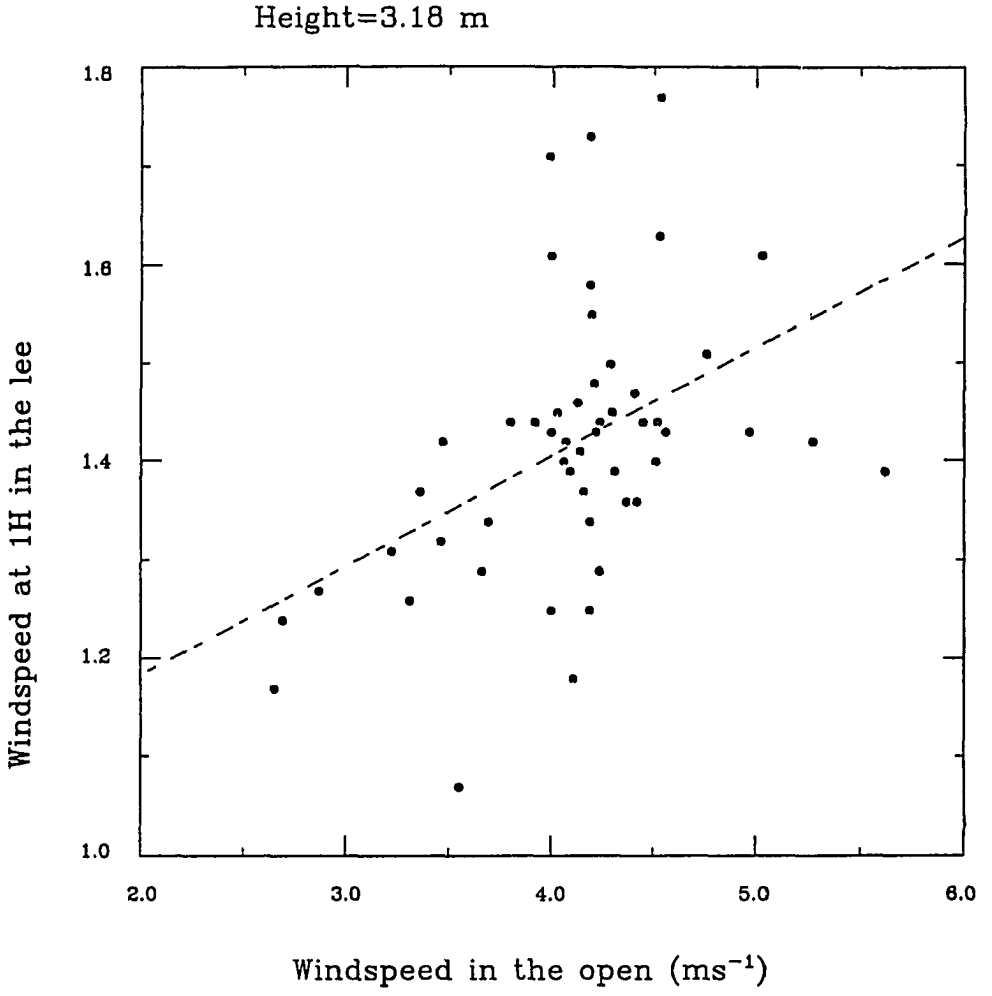

Fig. 11. Relationship between absolute windspeed in the open and windspeed in the lee of a shelterbelt at 3.18 m.

flow by turbulent processes. Shelterbelts, however, differ from one another in their physical structure according to species, spacing within a row and between rows, and stage of growth of the trees. Relative values of windspeed are often used to make comparisons between observations of wind-reduction effects of shelterbelts at different times and locations (Eimern et al. 1964). The windspeed profile upwind of the shelter is used to normalize observations in the lee. This implies that the windspeed reduction is assumed to be independent of the absolute value of the windspeed in the open. In fact this study indicates, in agreement with Eimern et al. (1964), that the windspeed in the lee is not independent of the windspeed in the open. Thus the normalization may lead to erroneous conclusions.

The regression analysis suggests a positive linear relationship between the windspeed in the open and the windspeed in the lee, measured at the same height. This means that the faster approach flows produce higher windspeed in the lee. According to Eimern et al. (1964), the absolute high windspeed in the open has no direct influence on the windspeed reduction, but the degree of permeability of shelterbelts could be altered by the strength of the undisturbed wind. A leafy deciduous shelterbelt seems to have higher porosity in higher winds since the leaves open more space as they are forced into a position parallel to the wind. For the

evergreen shelterbelts such as pine and juniper, however, the effect of the undisturbed flow strength on the reduced windspeed is opposite to that for deciduous. It was explained in the review by Eimern et al. (1964) that for the case of conifer shelterbelts the stronger wind reduces the permeability by forcing together the flat level branches like venetian blinds. As a result, the faster flow undergoes more reduction of its momentum by crossing a conifer shelterbelt. There is some disagreement, however, as to the threshold windspeed above which the shelterbelt density alteration becomes significant. Naegeli (1946) concluded that windspeeds as low as 2 m s^{-1} could cause a significant change in the belt permeability to the air flow, while the Denuyl (1936) measurements suggest that a significant alteration is observed at speeds over 5 m s^{-1}. In the present study we previously mentioned that the shelterbelt consisted of two rows of alternating pairs of ash and pine. The relationship between the windspeed in the open and the windspeed in the lee at 3.18 m, 5.18 m and 9.80 m is depicted in Fig. 11, Fig. 12 and Fig. 13 respectively. At the lower levels, Fig. 11 and Fig. 12 may suggest that for winds over 5 m s^{-1} the windspeed in the lee decreases with increasing windspeed in the open. There are only three data points where windspeed in the open is over 5 m s^{-1}, but this observation agrees with Denuyl (1936) measurements. The regression analysis is presented in

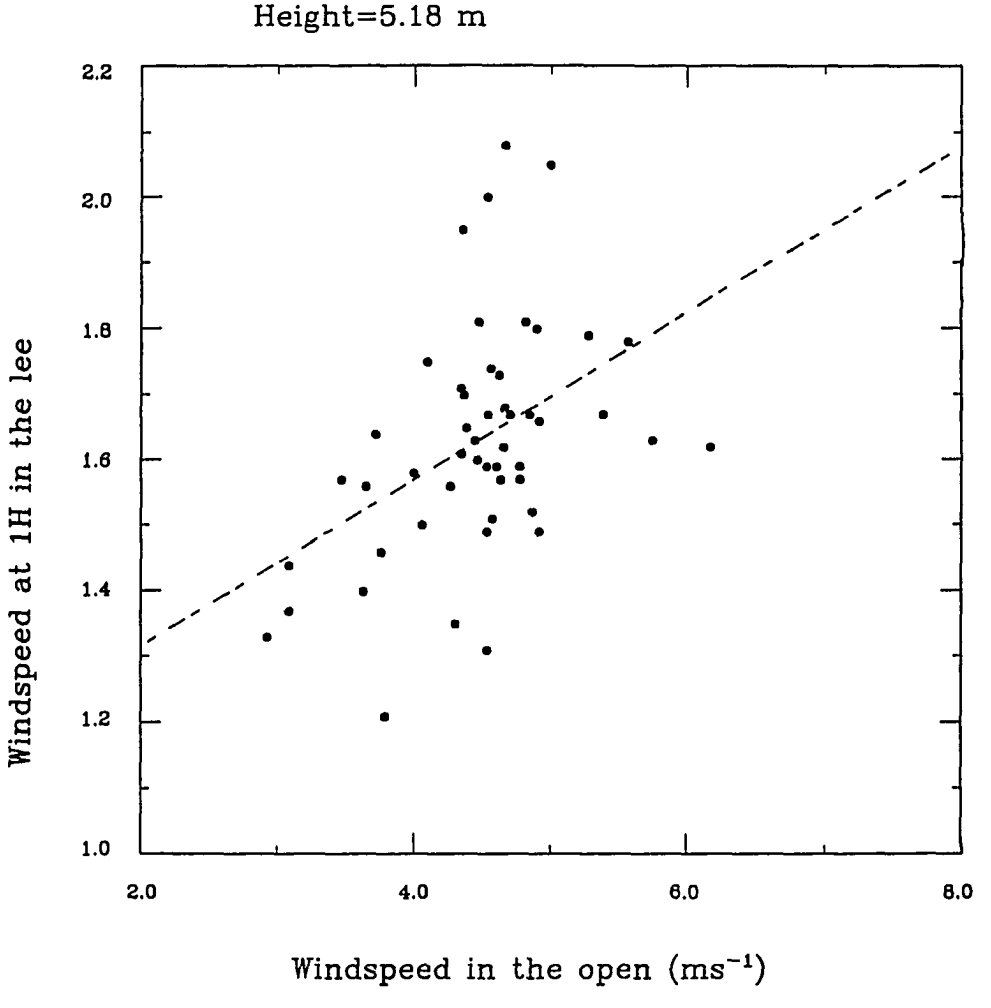

Fig. 12. Relationship between absolute windspeed in the open and windspeed in the lee of a shelterbelt at 5.18 m.

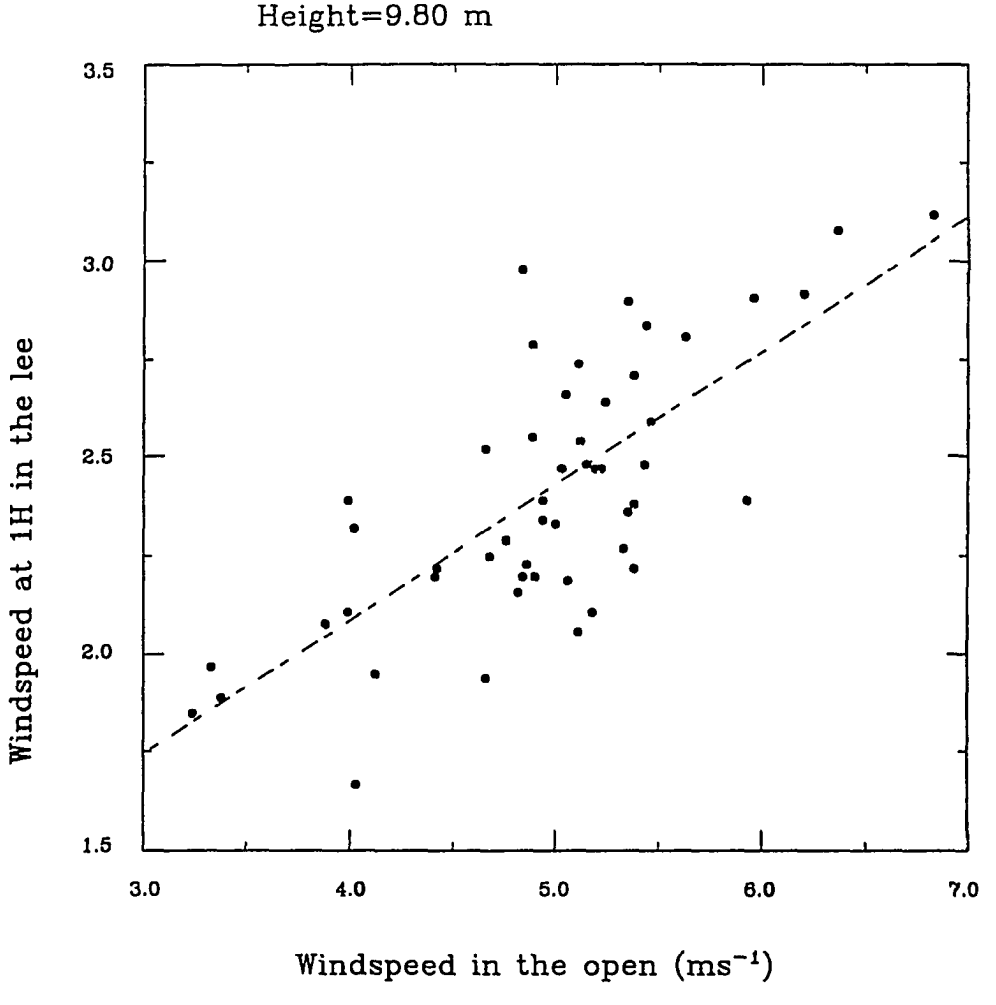

Fig. 13. Relationship between absolute windspeed in the open and windspeed in the lee of a shelterbelt at 9.80 m.

Table 1. The model explains little of the variability, mainly because most of it could be attributed to the effects of other variables, such as turbulence and static instability, that are not included in the regression model.

Table 1. Results of the regression analysis for Figs 11 through 13.

	Interc.	Slope	R^2	P-value	Height
Fig. 11	0.96	0.111	0.21	0.0006	3.18 m
Fig. 12	1.11	0.127	0.20	0.0009	5.18 m
Fig. 13	0.72	0.718	0.55	0.0020	9.80 m

2. Effect of the angle of incidence

For the influence of angle of incidence on reduced windspeed we expect as unlike the previous case a negative correlation as we know that when the velocity is oblique to the shelterbelt the distance travelled by the flow to cross the belt is longer than when the flow hits the belt perpendicularly. The width of the belt effectively increases, and for the same geometrical porosity and the same drag force an increase in shelter width has the same effect as an increase in shelter density (Takahashi, 1978). Thus the angle of incidence and the relative windspeed in the lee are negatively correlated (Fig. 14). The R^2 value is only 0.18 (Table 2) which suggests that there is much scatter, and this could be due to several reasons. First and foremost, for a

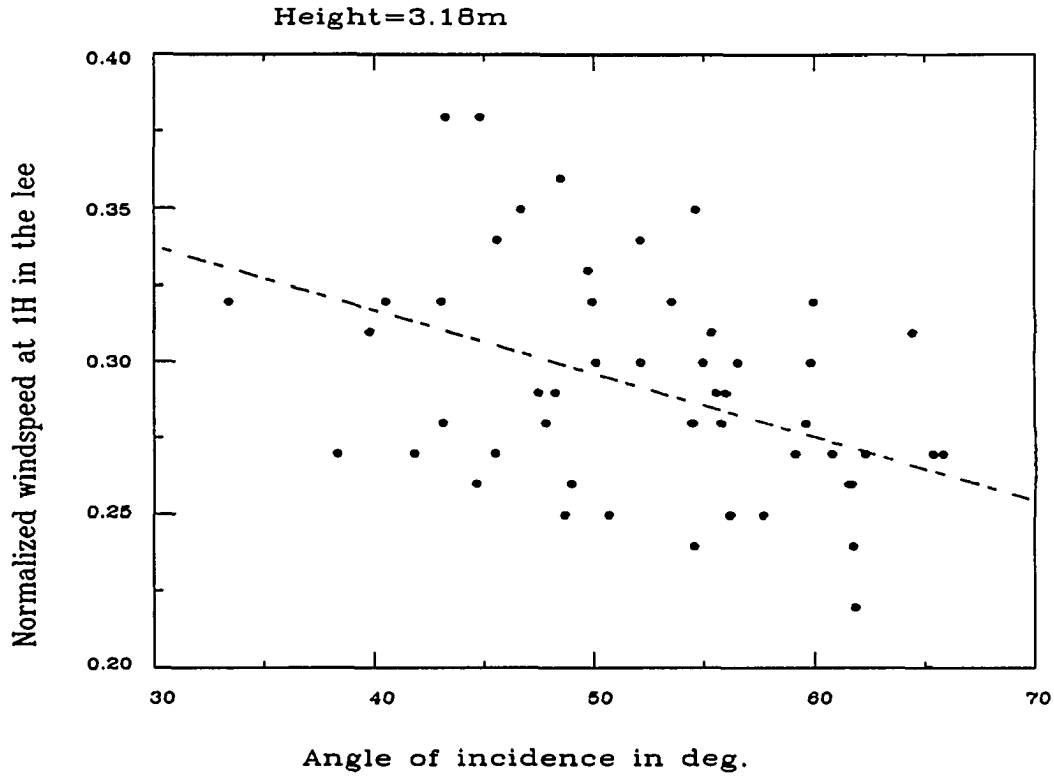

Fig. 14. Relationship between the angle of incidence of the undisturbed flow and the reduced windspeed in the lee at 3.18 m height.

Table 2. Results of the regression analysis for Figs 14 through 16.

	Interc.	Slope	R^2	P-value	Height
Fig. 14	0.40	-0.002	0.18	0.0001	3.18 m
Fig. 15	0.47	-0.003	0.22	0.004	5.18 m
Fig. 16	0.51	-0.0004	0.003	0.701	9.80 m

flow with an angle of incidence α, the distance travelled by the flow to cross the shelter will be Y such that $X \leq Y \leq X/\cos(\alpha)$ (X represents the width of the shelter). The pressure gradient, being perpendicular to the shelter, alters the direction of the flow by decreasing the wind angle with the normal to the belt. Also the magnitude of the pressure gradient across the shelter is strongly related to the undisturbed flow velocity. The faster free-stream flow generates a stronger pressure gradient, which in turn causes more deflection to the flow, resulting in a shorter distance Y. A shorter Y implies an increase of the porosity seen by the flow. Thus for the same angle of incidence, the faster flow produces less windspeed reduction. Thus the variability in the free stream velocity throughout the period (Fig. 10) is a possible cause for the scatter. Other influences not accounted for include the amount of turbulence in the approach flow and/or the air instability.

The effect of air instability on windspeed reduction in the lee of a windbreak was studied by Seginer (1975b). His findings indicated that the Richardson number was a two-valued function of the windspeed in the open and a significant dependence of the reduced windspeed in the lee on stability. Given the ability of the windspeed to alter the porosity of a shelterbelt, we thought that including the atmospheric stability as an independent variable in a multiple regression

analysis would not help. Guyot (1986) has studied the effect of mechanical turbulence in the approach flow on the windspeed reduction. His results suggest that the amount of turbulence in the approach flow diminishes the ability of a shelterbelt to reduce the flow momentum. We could not include this variable since it was not part of the measurements.

The analysis of the dependence sheltering effect on angle of incidence is repeated for data from 5.18 m (Fig. 15) and 9.80 m (Fig. 16). For details of the regression analysis refer to Table 2 where one can see at 9.80 m (toward the top of the trees) the relationship between reduced windspeed and angle of incidence is no longer significant. As indicated by the value of R^2 most of the variability is not explained by the model. At all three levels the results of the analysis led to the same conclusion as to how the reduced windspeed is related to the angle of incidence.

D. The Model

The aerodynamic model used in this study was first developed by Litvina (1987) at the Agrophysical Institute (Saint Petersburg, Russia). It is a two-dimensional model that solves a system of non-linear equations of velocity (u,w), and TKE (e) in the surface layer with closure based on the gradient-diffusion scheme. Shelterbelts are usually assumed to be uniform and have length at least an order of

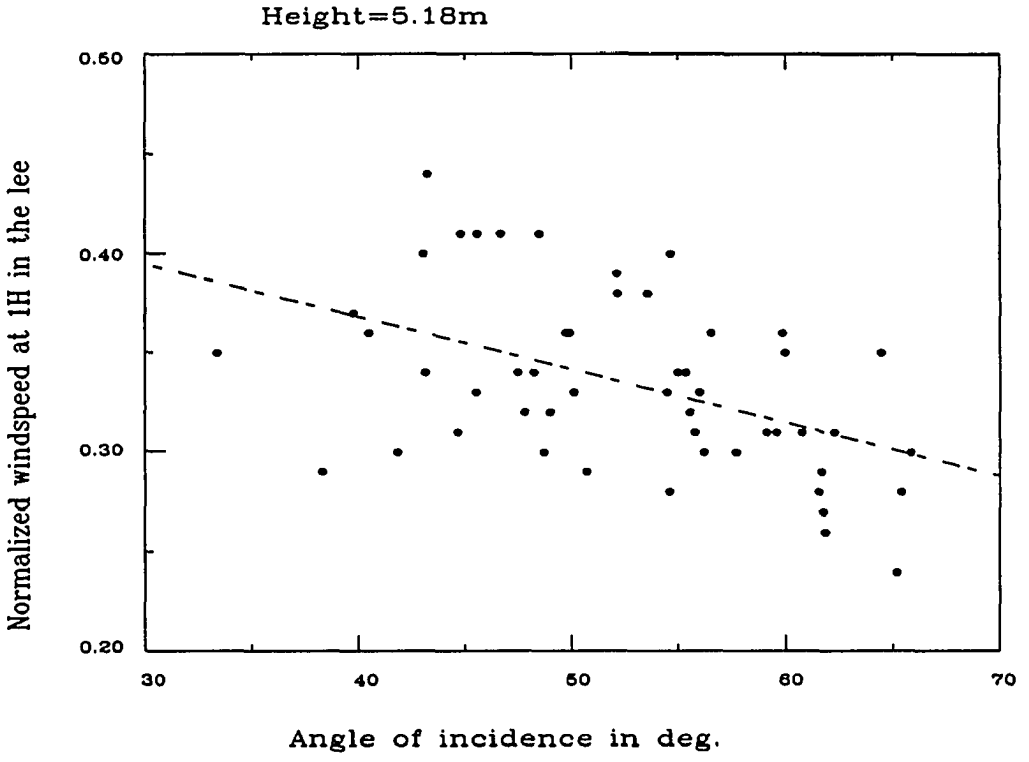

Fig. 15. Relationship between the angle of incidence of the undisturbed flow and the reduced windspeed in the lee at 5.18 m height.

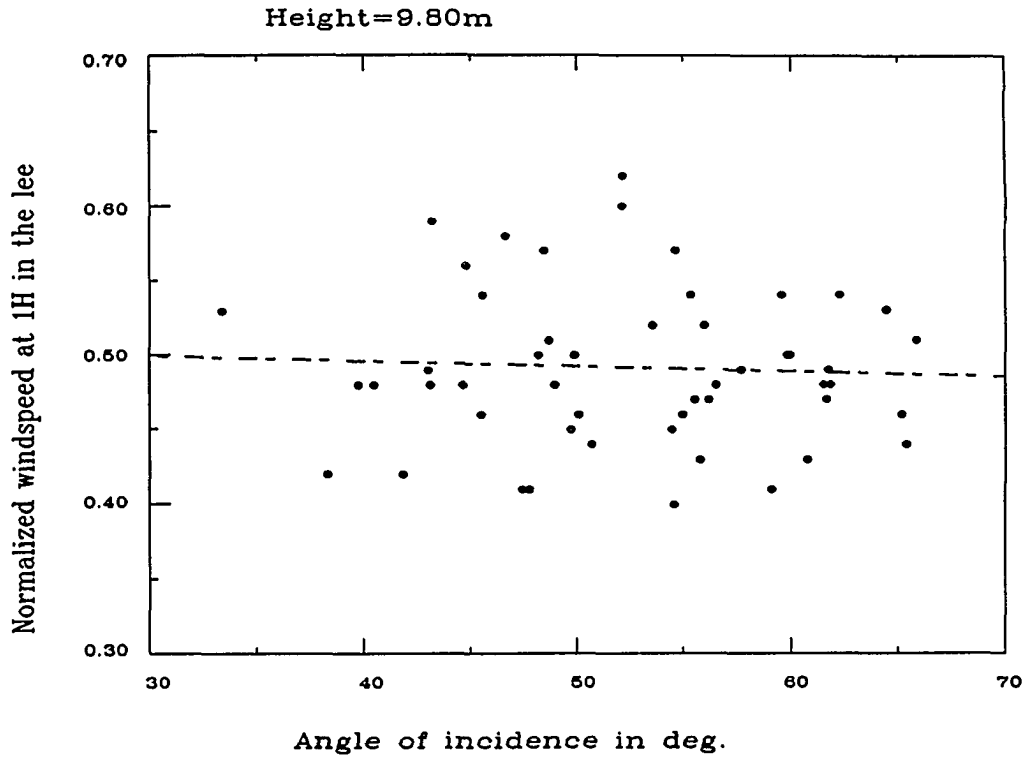

Fig. 16. Relationship between the angle of incidence of the undisturbed flow and the reduced windspeed in the lee at 9.80 m height.

magnitude larger than their height. The x-direction is taken to be perpendicular to the shelterbelt, and the z-direction is the vertical. The computational domain, used here, extends from the upwind edge of the shelterbelt to 20H downwind, and from the ground to 3H in the vertical. The horizontal grid spacing Δx is half of the shelter width up to the leeward edge of the shelter and $\Delta x = 0.5$ m thereafter. The vertical grid spacing Δz is constant from the ground to the top and $\Delta z = 0.1$ m.

Among the barrier properties that affect the flow are width, shape, height, and porosity (or, alternatively, the plant surface area per unit total volume), the latter two being most important (Bean et al., 1975; Borrelli et al., 1989; Hagen and Skidmore, 1971a). The effect of the barrier is described in the model by a drag force term in the momentum equation and by a corresponding source/sink term in the TKE equation. The horizontal component of the drag force is parameterized as:

$$F_x = C_f S u \frac{\sqrt{(u^2+w^2)}}{2} \tag{6}$$

The corresponding source term in the TKE budget equation is

$$F_x u = C_f S u^2 \frac{\sqrt{(u^2+w^2)}}{2} \tag{7}$$

These terms include both the drag coefficient C_f, and the plant surface area per unit total volume, S. The drag

coefficient relates the momentum extracted from a moving fluid by a body immersed in it to the maximum momentum that could be extracted by a body with equal cross-sectional area at right angles to the direction of the flow. For a shelterbelt the drag coefficient may be written as:

$$C_f = \frac{D}{0.5\rho u^2 H} \tag{8}$$

where D is the drag force per unit length evaluated with the momentum transfer method (Litvina and Takle, 1992):

$$D = \frac{\frac{1}{H}\int_0^H [P_W(z) - P_L(z)]\, dz}{0.5\rho u^2} \tag{9}$$

$P_W(z)=P_{SW} + 0.5\rho u_W^2$, and $P_L(z)=P_{SL} + 0.5\rho u_L^2$ are sums of static and dynamic local pressure windward (subscript W) and leeward (subscript L) respectively; u is the mean windspeed of the layer of thickness H.

The porosity, which is the ratio of the barriers open area surface to total surface, is accurately described by optical porosity for thin artificial fences. For wide natural barriers, however, the optical porosity derived through the use of photographic techniques is not equivalent to aerodynamic degree of permeability, because it shows only the two-dimensional gaps but not the three-dimensional spaces. To account for this difference, the specific surface of plant elements per unit volume S is used instead of the optical

porosity, where $S=\Delta s/\Delta V$, Δs being the plant elements surface and ΔV the volume these elements occupy in space. S increases with increasing density or decreasing porosity.

The vertical turbulent flux is parameterized as

$$-\overline{e'w'}=\alpha_e K\frac{\partial e}{\partial z} \tag{10}$$

where $\alpha_e=0.73$ is a constant that accounts for an adjustment for atmospheric boundary-layer flow (Litvina and Takle, 1992).

1. The equations

The equations will include the momentum equation, the continuity equation, and TKE equation.

Momentum equation:

$$u\frac{\partial u}{\partial x}+w\frac{\partial u}{\partial z}=\frac{\partial}{\partial z}\left(K\frac{\partial u}{\partial z}\right)-C_f Su\frac{\left(u^2+w^2\right)^{1/2}}{2} \tag{11}$$

Turbulent kinetic energy equation:

$$u\frac{\partial e}{\partial x}+w\frac{\partial e}{\partial z}=\frac{\partial}{\partial z}\left(\alpha_e K\frac{\partial e}{\partial z}\right)+K\left(\frac{\partial u}{\partial z}\right)^2+C_f Su^2\frac{\left(u^2+w^2\right)^{1/2}}{2}-\frac{C_1 e^2}{K} \tag{12}$$

Continuity equation:

$$\frac{\partial u}{\partial x}+\frac{\partial w}{\partial z}=0 \tag{13}$$

where:

u horizontal component of the wind speed

w the vertical component

e the turbulent kinetic energy

K is the eddy diffusivity

C_f is the drag coefficient

For the sake of numerical stability the equations are solved for u_1 and e_1, which are the departures from the corresponding values of the approach flow u_0 and e_0 such that: $u=u_0 + u_1$ and $e=e_0 + e_1$ with $u_0=\frac{u_*}{k}\ln\left(\frac{z+z_0}{z_0}\right)$ and $e_0=C_1^{-1/2}u_*^2$ where u_* and z_0 are the friction velocity and the roughness height, respectively, and k the von Karman constant.

The last term in the TKE equation represents the dissipation, while the one before it simulates the production of TKE by the shelter through momentum extraction from the mean flow.

2. Model numerics

The equations are put in the following form (see Appendix A for intermediate steps):

$$a\frac{\partial f}{\partial x}+b\frac{\partial f}{\partial z}=\frac{\partial}{\partial z}\left(c\frac{\partial f}{\partial z}\right)+d+gf \qquad (14)$$

where f represents the variable u_1 for the momentum equation, and b_1 for the TKE equation. The coefficients a=u, b=w, c=K The resulting finite-difference form is

$$\left.\begin{aligned} a_{i-1/2,j}\frac{f_{ij}-f_{i-1,j}}{\Delta x}+b_{i-1/2,j}\frac{f_{i,j+1}-f_{i,j-1}}{2\Delta z}= \\ +\frac{1}{\Delta z^2}\left[c_{i-1/2,j+1/2}\left(f_{i,j+1}-f_{i,j}\right)\right] \\ -\frac{1}{\Delta z^2}\left[c_{i-1/2,j-1/2}\left(f_{i,j}-f_{i,j-1}\right)\right] \\ +d_{i-1/2,j}+g_{i-1/2,j}f_{i,j} \end{aligned}\right\} \tag{15}$$

or

$$\left.\begin{aligned} \left(-\frac{b_{i-1/2,j}}{2\Delta z}-\frac{c_{i-1/2,j-1/2}}{\Delta z^2}\right)f_{i,j-1}+\left(\frac{a_{i-1/2,j}}{\Delta x}+\frac{c_{i-1/2,j+1/2}}{\Delta z^2}\right)f_{i,j}+ \\ \left(\frac{c_{i-1/2,j-1/2}}{\Delta z^2}-g_{i-1/2,j}\right)f_{i,j}+\left(\frac{b_{i-1/2,j}}{2\Delta z}-\frac{c_{i-1/2,j+1/2}}{\Delta z^2}\right)f_{i,j+1}= \\ \frac{a_{i-1/2,j}}{\Delta x}f_{i-1,j}+d_{i-1/2,j} \end{aligned}\right\} \tag{16}$$

but

$$\left.\begin{aligned} c_{i-1/2,j-1/2}=0.5\left(c_{i-1/2,j}+c_{i-1/2,j-1}\right) \\ c_{i-1/2,j+1/2}=0.5\left(c_{i-1/2,j+1}+c_{i-1/2,j}\right) \end{aligned}\right\} \tag{17}$$

which lead to

$$c_{i-1/2,j-1/2}+c_{i-1/2,j+1/2}=\frac{1}{2}\left(c_{i-1/2,j-1}+2c_{i-1/2,j}+c_{i-1/2,j+1}\right) \tag{18}$$

Eq. 16 can be written as

$$\alpha_j f_{i,j-1}+\beta_j f_{i,j}+\gamma_j f_{i,j+1}=\delta_j \tag{19}$$

with

$$\alpha_j=-\frac{1}{2\Delta z}\left(b_{i-1/2,j}+\frac{1}{\Delta z}\left(c_{i-1/2,j}+c_{i-1/2,j-1}\right)\right) \tag{20}$$

$$\beta_j = \left\{ \left(\frac{d_{i-1/2,j}}{\Delta x} + \frac{(c_{i-1/2,j-1} + 2c_{i-1/2,j} + c_{i-1/2,j+1})}{2\Delta z^2} \right) - g_{i-1/2,j} \right\} \tag{21}$$

$$\gamma_j = \left(\frac{b_{i-1/2,j}}{2\Delta z} - \frac{(c_{i-1/2,j+1} + c_{i-1/2,j})}{2\Delta z^2} \right) \tag{22}$$

$$\delta_j = \frac{a_{i-1/2,j}}{\Delta x} f_{i-1,j} + d_{i-1/2,j} \tag{23}$$

The numerical scheme of Eq. 19 is fully implicit and algebraically non-linear due to the appearance of quantities unknown at the i level in the coefficients. The linearization is done by simple iterative update of the coefficients. That is, the coefficients are first evaluated at the i-1 level (lagged) and the system solved at the i level. The coefficients are then updated by utilizing the solution just obtained at the i level. The iteration continues until convergence is achieved.

Usually the Thomas algorithm is used to solve the system generated by Eq. 19. In order to save computer storage space a better alternative is employed, whereby the use of Thomas algorithm is avoided. Through algebraic manipulations and the use of the boundary conditions, Eq. 19 could be cast in the following form (the "i" index is dropped, because the equation is solved vertically before a streamwise increment is performed).

$$f_j=A_jf_{j+1} + B_j \tag{24}$$

It can be shown that the coefficients A_j and B_j can be computed from bottom to top in terms of known quantities according to the following formulae (see Appendix A for details).

$$A_j=\frac{-\gamma_j}{\beta_j+\alpha_jA_{j-1}} \qquad B_j=\frac{\delta_j-\alpha_jB_{j-1}}{\beta_j+\alpha_jA_{j-1}} \tag{25}$$

Once the coefficients are determined, we can use the top boundary condition, and work the solution from top to bottom with the aid of Eq. 24 for j=N,N-1,N-2,.....,1

3. Boundary condition

At x=0 $u=\frac{u_*}{k}\ln\left(\frac{z+z_0}{z_0}\right)$; w=0; $K=ku_*(z+z_0)$; $e=e_0$

At z=0, u=w=0; $\alpha_e K\frac{\partial e}{\partial z}=0$; $l=kC_1^{1/4}z_0$

At the top of the domain $K\frac{\partial u}{\partial z}=u_*^2$; $\alpha_e K\frac{\partial e}{\partial z}=0$

$\alpha_e=0.73$ and $C_1=0.046$ are both constants suggested by Laikhtman cited in Litvina and Takle (1992).

4. The closure

To close the system, the Kolmogorov relationships were employed:

$K=l\sqrt{e}$ and $\epsilon=C_1\frac{e^2}{K}$

The turbulent length scale is given by:

$$\frac{1}{l}=-\frac{1}{kC_1^{1/4}}\frac{\frac{\partial}{\partial z}\left(\frac{e}{K}\right)}{\frac{e}{K}}+\frac{S}{A} \tag{26}$$

The first term of Eq. 26 describes the well known Karman idea of connecting local characteristics to the length scale; the second term, where A=0.2, describes the impact of plant structure for a uniform crop (see Appendix A for the discretized form of K).

E. Tuning and Testing of the Model

Numerical models are obviously invaluable tools that help solve fluid mechanics problems at a lesser cost than field experiments. It will be tempting to say as it is customary in the numerical modeler jargon, that a model needs to be validated before it is used for applications. According to Oreskes et al. (1994), however, the term validation has been erroneously used. It has been used synonymously with verification. The term validation has also been misleadingly used to suggest that the model is an accurate representation of physical reality. When validation is used as synonymous of verification, Oreskes at al. argued that a numerical model veracity can never be established. Verification is only possible with closed systems. Although numerical models may contain closed mathematical components, they are not closed systems because they are loaded with assumptions, approximations, input parameters and data that are only partially known. Oreskes at al. (1994) asserted that, while many inferences and assumptions can be justified on the basis

of experiments, the degree to which these assumptions hold in any new study can never be established a priori. Based on these arguments we could say that closure applied in atmospheric turbulence is a good example of approximation that leaves the system open. In our case here it is appropriate to say that experimental data will be used to evaluate or test the model performance.

The Mead (Nebraska) Field Experiment provided the vertical wind profiles that were used to evaluate the model. The model is a diagnostic one that assumes a neutrally stratified atmosphere. We, therefore, need to select those profiles that are consistent with neutral stratification. The data are divided into sets that combine several 5-min runs each. Profiles of set averages are plotted in Fig. 17 and Fig. 18. Fig. 17 shows that on Julian day 264 (first day of the experiment) profiles from the four sets are indicative of a slightly stable atmosphere. These are not suitable for model testing. Luckily, Fig. 18 shows profiles that are consistent with neutral or near neutral stratification.

These profiles are used as boundary conditions to run the model for comparison between the simulations and observations in the lee of the shelterbelt. The sensors are at ten different heights that extend from the ground up to 10 m (Table 3), but the model has a higher resolution (one grid point every 10 cm). In order to get an upwind profile as a

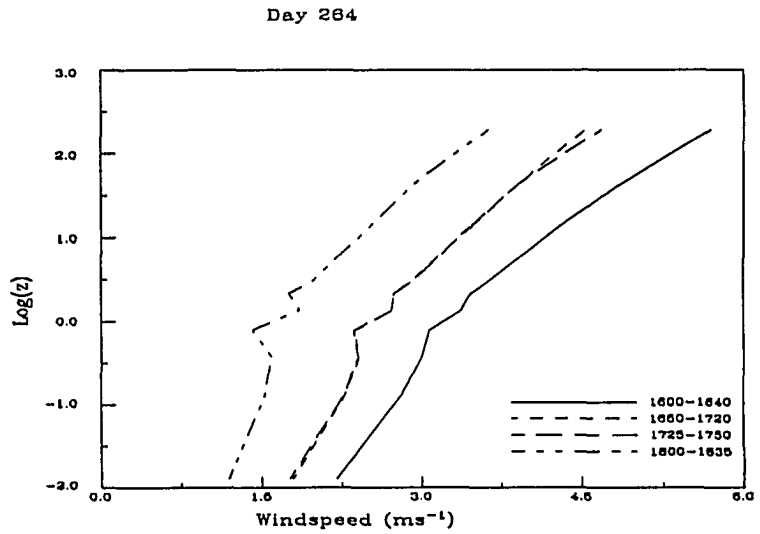

Fig. 17. Upwind vertical profiles of horizontal wind consistent with stable conditions.

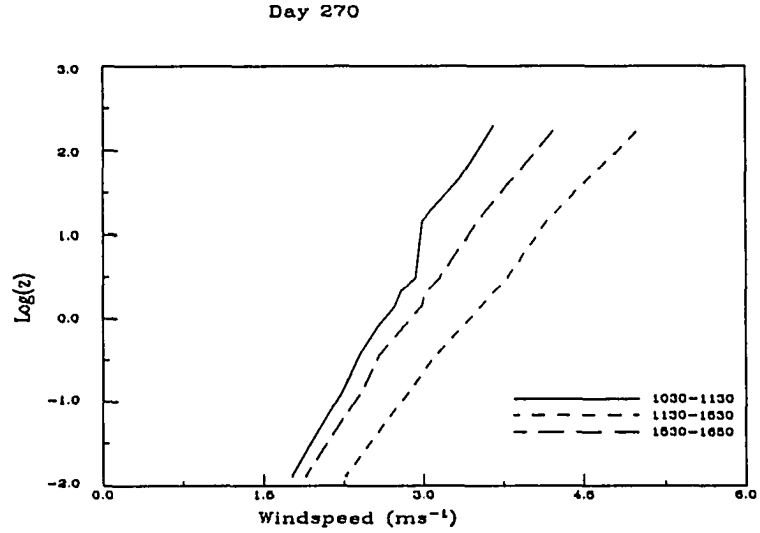

Fig. 18. Upwind vertical profiles of horizontal wind consistent with neutral stratification.

Table 3. Cup-anemometer and thermistor heights (m) for the three observation masts.

Level	Mast 1	Mast 2	Mast 3
1	0.15	0.35	0.15
2	0.41	0.57	0.40
3	0.65	0.84	0.65
4	0.90	1.09	0.90
5	1.15	1.32	1.16
6	1.39	1.57	1.41
7	1.63	1.83	1.68
8	3.18	3.35	3.18
9	5.18	5.35	5.18
10	9.80	9.97	9.80

model boundary condition that also fits the observations, the upwind observed profiles are used to compute z_0 and u_* (for computation details see Appendix B). These two parameters are then used to generate the reference profile. Furthermore, within these sets only windspeed larger than or equal to 3 m s^{-1} at the top of mast 1 were considered for the averages, because higher winds generate more mechanical turbulence. The eddy mixing will result in reduced gradients.

1. Tuning of the model

A preliminary comparison of the experimental windspeed profiles and those simulated by the model failed, because the simulations overestimated the recovery rate. The original version of the model, however, was satisfactorily tested against data taken in the lee of a relatively shorter shelterbelt consisting mainly of annual crops (Litvina and Takle, 1992). At the University of Nebraska Shelterbelt Facility the tree belt height was estimated at 12 m during the time of the experiment. This height was an order of magnitude larger than the height of annual crop shelterbelts used originally.

Data from field experiment and wind-tunnel tests showed that besides permeability effects, the shelterbelt and windbreak drag increases with an increase in the ratio H/z_0, or an increase in shelter height relative to the effective roughness (Raine and Stevenson, 1977). Consequently Plate (1971) suggested a drag law of the form $C_f=C\ln(H/z_0) + D_1$, where C_f is the drag coefficient, and C and D_1 are constants. Raine and Stevenson stated that although the drag law was first derived for impermeable barriers mounted on a smooth wall (wind tunnel), it was quite relevant to the fully aerodynamically rough flows mostly found in nature. The drag-law relationship suggests that the smoother the surface on which a windbreak is erected, the greater will be the

windspeed reduction in the lee. An increase in height that is not followed by a proportional increase in the roughness height, also will cause a larger drag and will have the same effect on the windspeed reduction as smoothing of the surface. The data by Naegeli (1946) and Panfilov (1948), both reported in Eimern et al. (1964), indicate that for low to medium shelter density, a drag increase implies more windspeed reduction all the way downwind to the point of full recovery.

The fact that the shelterbelt height for trees is an order of magnitude larger than for crops is, thus, the likely reason for the poor performance of the model; in other words the model was not designed for such large H/z_0. As was stated previously, a change in shelter height induced a change in shelter drag force. The drag force was in turn related to the perturbed pressure field on both sides of the shelterbelt (Plate, 1971). Thus, the reason the model did not agree with observations for large H/z_0 was because the momentum equation did not have a pressure gradient term. Fixing this problem in a physically sound manner is not an easy task. In fact, Plate (1971) stated that the main difficulty in predicting shelter drag forces stemmed from our inability to determine the base pressure in the lee of solid barriers and the pressure gradients along a perpendicular to the shelter for porous ones.

In order to remedy this deficiency, the lack of a

pressure gradient term in the momentum equation is compensated by the drag force term (Eq. 6). Originally this term is made to vanish at and beyond the lee edge of the belt. Here, we use it to account for the pressure gradient term since it consists of the drag coefficient, the shelter density, and the windspeed in the lee, which are all related to the pressure field around a shelterbelt. Knowing that the pressure gradient caused by the shelter vanishes somewhere in the lee, we made the drag term decrease from its value at the lee edge to zero at 5H downwind from the shelter by multiplying it by $1-\frac{X-W}{5H}$ where X and W are the leeward horizontal distance and the belt width, respectively. As empirical as it may look, this adjustment has tremendously decreased the rate of recovery, and allowed good agreement between observations and simulations in general.

This tuning, however, put some restrictions as to the future use of the model. The experimental data only covered the near lee. Had data been available in the far lee, the outcome of the tuning would have been different. The simulations are also affected by the ratio H/z_0, so for different roughness height or different shelter height another tuning is necessary. This, however, does not affect the usefulness of the model, additional testing against profiles at other locations in the lee and testing against other shelters are necessary if the model is to be used for general

application to shelterbelts.

2. Search for the best porosity parameter S

The porosity parameter S was not measured in the field. For the tuning of the model in the previous section, S was found using a visual estimation performed on plots for several values of S (Figs. 19 and 20). The value that minimizes departures between the observation points and the simulation curves is chosen to represent the structure of the shelterbelt. In order to have a porosity parameter S that best describes the shelterbelt internal structure, we compare the differences between observations and simulations by a quantitative method.

A measure of the overall departure of simulations from observations is obtained by taking the square root of the sum of squares of weighted departures at all measurement levels:

$$\overline{W_e}=\sqrt{\sum_i w_i (w_{si}-w_{mi})^2} \qquad (27)$$

where w_{si} and w_{mi} are, respectively, the simulated and measured windspeeds at level i, and w_i is a weight. This weight is introduced for two reasons: 1) there are more observation points in the lower part, and 2) departure magnitude does not have the same significance at low and high levels (e. g. at high levels the windspeed is higher than near the surface and a large departure at high levels could be relatively small).

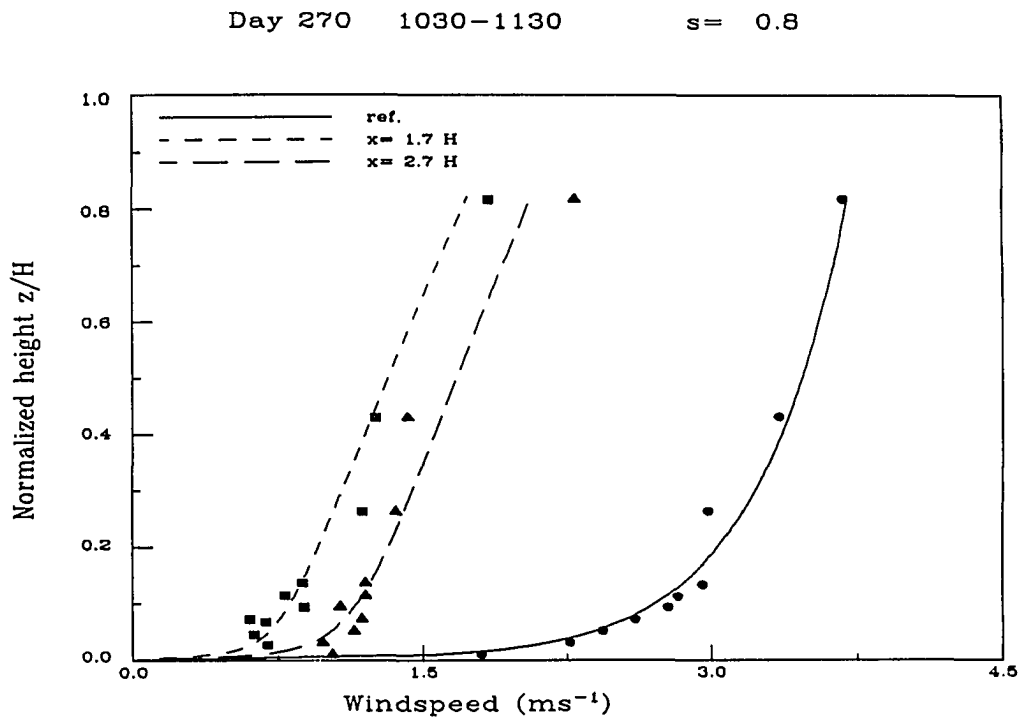

Fig. 19. Simulated and measured profiles. Symbols represent measurements: upwind •, in the lee ■ at 1H and ▲ at 2H. Set 1 (10:30-11:30).

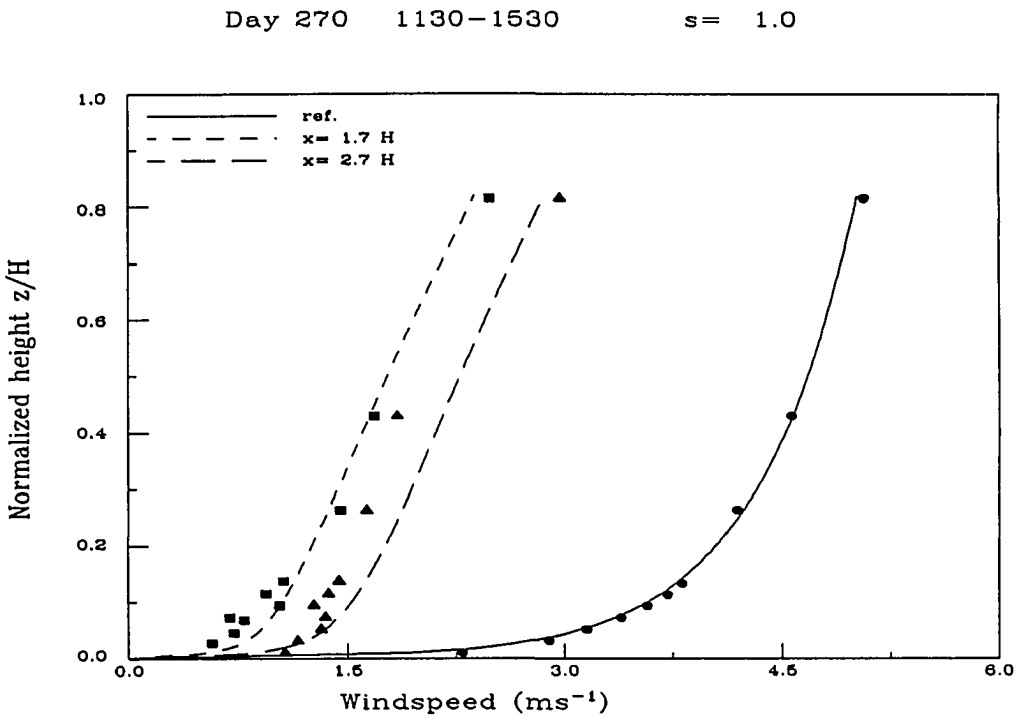

Fig. 20. Simulated and measured profiles. Symbols represent measurements: upwind •, in the lee ■ at 1H and ▲ at 2H. Set 2 (11:30-15:30).

Two simulations were run to obtain two wind profiles, the first with S=0.4 (low density) and the second with S=1.8 (high density). Differences between values from the two profiles were computed at each level. The ratio of the square of this difference to the difference in height between two consecutive observation points is used to compute the weight as follows.

$$w_i = \frac{(\Delta z)_i}{(\delta u)^2_i} \quad where (\Delta z)_i = z_i - z_{i-1}; \quad (\delta u)_i = (u_{0.4} - u_{1.8})_i \tag{28}$$

The difference between observations and simulations is computed for a given value of S and normalized by the difference in simulated wind speeds for S=0.4 ($u_{0.4}$) and S=1.8 ($u_{1.8}$). This will give departures at all levels the same weight; otherwise departures at high levels will be larger than the ones at low levels. The overall sum of departures is, therefore, computed using Eq. 27 for S varying from 0.4 to 1.8. The results are plotted in Fig. 21 and summarized in Table 4. Note that for the 1030-1130 set the minimum of $\overline{W_e}$ is at S=0.6, whereas it is at about S=1 for the other sets. The 1030-1130 set wind speeds are weaker than for the other sets, and the effect of windspeed on S has been studied in the previous sections. It is expected that weak winds cause our shelterbelts to behave as if it were more porous and, therefore, have a smaller S.

When $\overline{W_e}$ is divided by $n\sum_i \Delta z_i$ (n is the number of

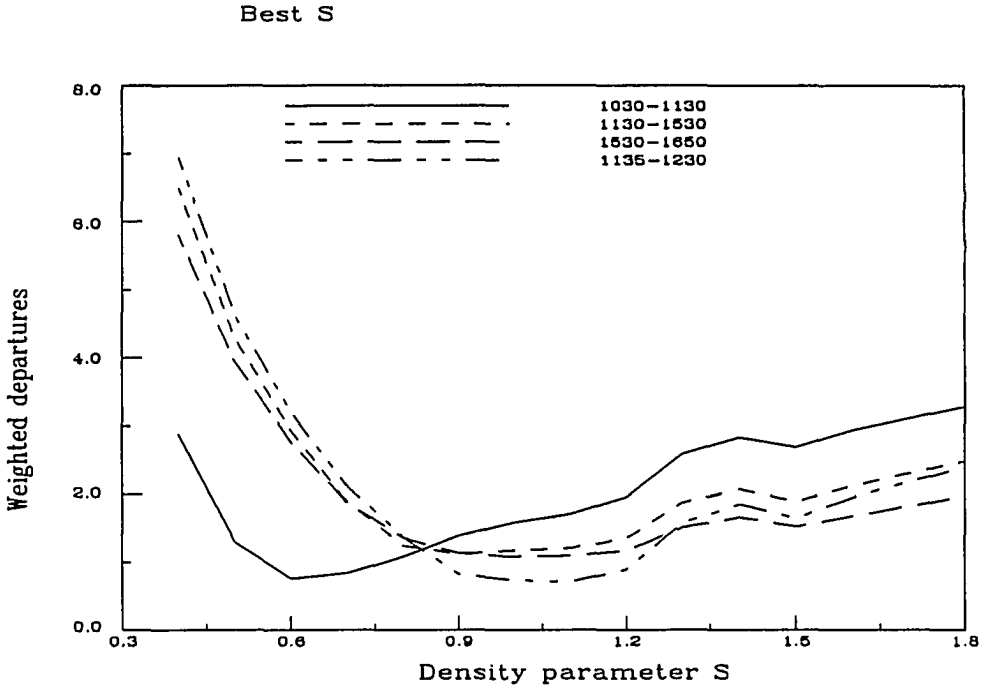

Fig. 21. Departures of simulations from observations based on table 2.

Table 4. Values of overall departures of model wind-speeds from observations for various values of S in simulations.

S	1030-1130	1130-1530	1530-1630	1135-1230
0.4	2.87	6.48	5.80	6.94
0.5	1.30	4.30	3.95	4.64
0.6	0.76	2.94	2.77	3.21
0.7	0.84	1.89	1.97	2.11
0.8	1.08	1.24	1.36	1.37
0.9	1.39	1.12	1.13	0.82
1.0	1.58	1.17	1.08	0.73
1.1	1.71	1.21	1.09	0.71
1.2	1.96	1.35	1.17	0.89
1.3	2.59	1.88	1.51	1.58
1.4	2.83	2.07	1.66	1.85
1.5	2.69	1.89	1.52	1.65
1.6	2.94	2.12	1.68	1.95
1.7	3.11	2.30	1.82	2.18
1.8	3.28	2.48	1.97	2.39

measurement points), it will yield an average relative departure that will be used a quantitative criterion for model performance evaluation. If this relative average departure is less than 0.015, meaning that the average absolute departure is less than 1.5% of the difference between simulated values at low (S=0.4) and high density (S=1.8), the model performance is satisfactory. If this departure is less than 1% then the model performance is very satisfactory. In our case $n\Sigma\Delta z_i=98$,

and for the best S (Table 4) the simulations of the 1030-1130 and 1135-1230 sets were very satisfactory, because the relative average departures are 0.8% and 0.7%, respectively.

3. Model testing

The upwind observed profile for set 1 (10:30-11:30) does not fit the computed logarithmic profile as well as the others (see curve "ref." and the corresponding observed data points of Fig. 22 and Table 5). The closest simulation profiles to the observations were obtained with the porosity parameter S=0.6. Our study of the relationship of angle of incidence to reduced windspeed earlier in this section showed that these two variables are negatively correlated, meaning that the reduced windspeed in the lee behaved as if the higher angle of incidence played the role of higher density (less porosity). For the period when set 1 (10:30-11:30) is recorded, Fig. 9 showed an average incidence angle of about 45°. This was the smallest angle of incidence for the whole day, except for a short period around 13:00. Set 2 (11:30-15:30) has the largest average incidence angle (55°). A larger incidence angle has the effect of a larger shelter density, which translates into a larger S for the simulations. S is indeed larger for set 2 than for the other sets, as shown in Fig. 23 and Table 6 where the profiles at 1H and 2H from the edge of the shelter downwind fit well. For the set 3 (15:30-16:50),

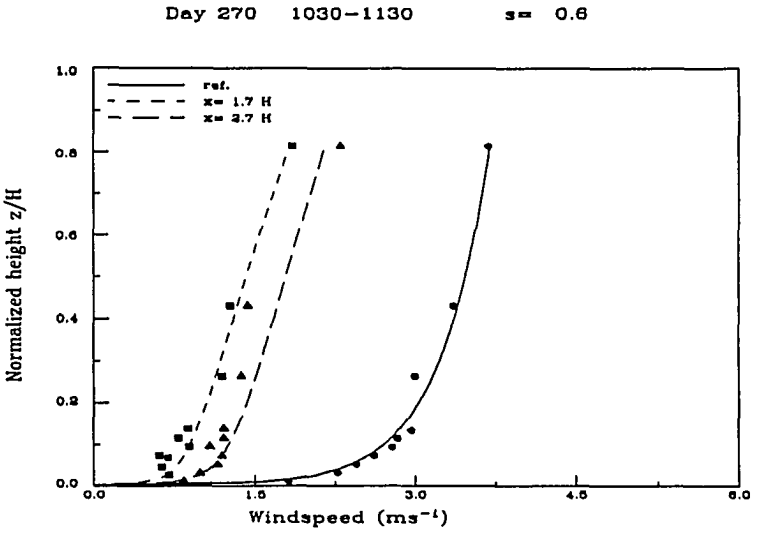

Fig. 22. Simulated and measured profiles. Symbols represent measurements: upwind •, in the lee ■ at 1H and ▲ at 2H. Set 1 (10:30-11:30).

Table 5. Observed values of Fig. 22 (U) and their standard errors (S.E.). From bottom to top.

Upwind		1H leeward		2H leeward	
U	S. E.	U	S. E.	U	S. E.
1.78	0.07	0.67	0.15	0.80	0.14
2.24	0.10	0.60	0.05	0.95	0.11
2.41	0.12	0.66	0.06	1.11	0.12
2.58	0.13	0.58	0.05	1.15	0.12
2.75	0.13	0.86	0.07	1.04	0.14
2.80	0.15	0.76	0.06	1.17	0.14
2.93	0.13	0.85	0.07	1.17	0.14
2.96	0.28	1.16	0.06	1.33	0.13
3.32	0.23	1.23	0.09	1.39	0.11
3.65	0.23	1.82	0.13	2.26	0.16

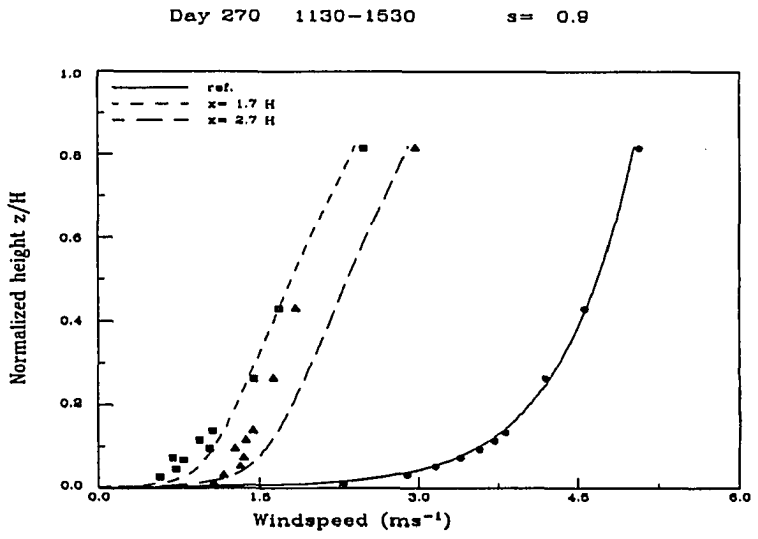

Fig. 23. Simulated and measured profiles. Symbols represent measurements: upwind •, in the lee ■ at 1H and ▲ at 2H. Set 2 (11:30-15:30).

Table 6. Observed values of Fig. 23 (U) and and their standard errors (S.E.). From bottom to top.

Upwind		1H leeward		2H leeward	
U	S. E.	U	S. E.	U	S. E.
2.26	0.04	0.54	0.01	1.03	0.04
2.86	0.04	0.69	0.02	1.12	0.05
3.12	0.05	0.76	0.02	1.28	0.05
3.36	0.06	0.66	0.02	1.31	0.05
3.54	0.06	1.00	0.02	1.23	0.06
3.68	0.06	0.91	0.02	1.33	0.05
3.78	0.06	1.03	0.02	1.40	0.05
4.16	0.07	1.42	0.02	1.59	0.05
4.53	0.08	1.65	0.03	1.80	0.06
5.03	0.09	2.45	0.05	2.93	0.06

however, (Fig. 24 and Table 7) it was impossible to make the simulations fit the observations for mast 1 and mast 2 simultaneously by varying S. At 4.18-m and 5.18-m of heights the windspeed at the further mast is lower than at the closer one. This suggests that the maximum windspeed reduction occurred beyond the mast closest to the shelter at 1H from the edge. A further investigation took us back to Fig. 10. It was observed that the windspeed reduction is more sensitive to changes of the approach flow windspeed at 2H than at 1H: the changes in reduced windspeed in response to changes in the upwind velocity are relatively large at 2H than 1H. Thus every time the windward undisturbed flow undergoes an steady decrease in speed, the reduced windspeed at 2H goes below that at 1H. Fig. 10 shows a decrease in the undisturbed flow speed for a good portion of the period 15:30-16:50, starting around 16:00. During the same time the speed at 2H remained lower than at 1H. As demonstrated by the data of Hagen and Skidmore, the position of minimum windspeed moved leeward as windbreak porosity increased. We have shown previously that when the windspeed in the open decreases, the shelterbelt acts as if it is more porous. In our case here, the windspeed decrease resulted in a porosity increase, which in turn caused the minimum windspeed to move leeward to be approximately centered at 2H. The model, however, is not able to capture the motion of the minimum position with respect to porosity

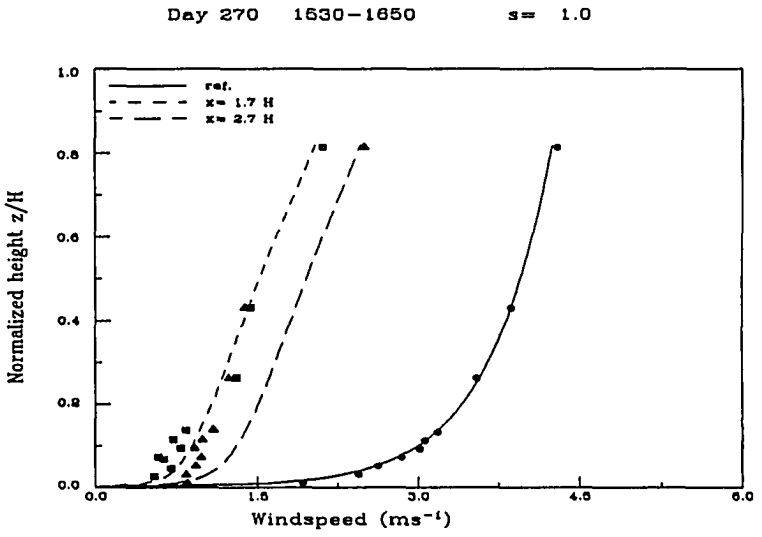

Fig. 24. Simulated and measured profiles. Symbols represent measurements: upwind •, in the lee ■ at 1H and ▲ at 2H. Set 3 (15:30-16:50).

Table 7. Observed values of Fig. 24 (U) and and their standard errors (S.E.). From bottom to top.

Upwind		1H leeward		2H leeward	
U	S. E.	U	S. E.	U	S. E.
1.89	0.09	0.51	0.01	0.81	0.09
2.41	0.11	0.67	0.13	0.80	0.09
2.59	0.13	0.60	0.03	0.89	0.11
2.81	0.14	0.55	0.02	0.94	0.11
2.98	0.14	0.76	0.04	0.88	0.11
3.03	0.16	0.69	0.04	0.95	0.11
3.15	0.15	0.81	0.05	1.05	0.11
3.51	0.17	1.27	0.05	1.19	0.11
3.83	0.18	1.40	0.06	1.34	0.12
4.26	0.21	2.08	0.10	2.46	0.14

change. The simulations indicate the presence of a secondary minimum for S higher than 2, the primary minimum remains always close to the shelter, which is in agreement with Raine and Stevenson (1977) observations. The reason resides in the fact that the momentum sink term is caused to vanish at the lee edge of the shelterbelt. When only runs with windspeed greater than or equal to 5 m s^{-1} are considered for the averages the agreement between model and observations gets even better (Fig. 25 and Table 8).

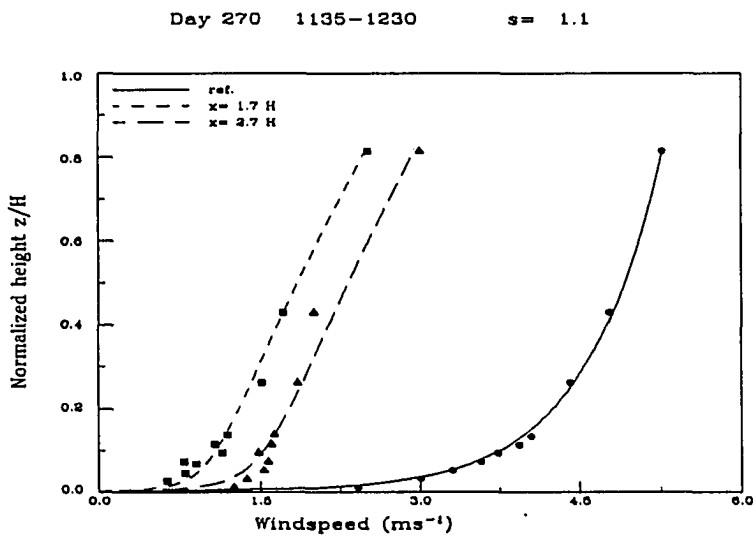

Fig. 25. Simulated and measured profiles. Symbols represent measurements: upwind •, in the lee ■ at 1H and ▲ at 2H. Stronger winds (≥5 m/s).

Table 8. Observed values of Fig. 25 (U) and and their standard errors (S.E.). From bottom to top.

Upwind		1H leeward		2H leeward	
U	S. E.	U	S. E.	U	S. E.
2.38	0.03	0.60	0.04	1.21	0.08
2.97	0.04	0.77	0.05	1.33	0.09
3.27	0.04	0.87	0.05	1.49	0.11
3.54	0.04	0.76	0.05	1.53	0.11
3.70	0.05	1.11	0.04	1.44	0.13
3.90	0.05	1.04	0.04	1.56	0.12
4.01	0.05	1.16	0.05	1.59	0.12
4.38	0.06	1.48	0.05	1.81	0.13
4.74	0.06	1.68	0.06	1.96	0.14
5.23	0.05	2.48	0.06	2.96	0.09

III. WINDSPEED REDUCTION IN THE LEE OF POROUS SHELTERS

A. Windspeed Reduction as a Function of Leeward distance and Shelter Density

After having been tested, the model performance on simulating wind profiles in the lee of shelterbelts was found satisfactory. We could therefore use the model with confidence to run experiments, for which experimental data don't exist. Comparisons between different field experiments on shelterbelts are made easier by use of dimensionless quantities. Thus, the dimensionless heights (η) and the horizontal distances (ζ) will be expressed in terms of shelter height: $\zeta = x/H$, $\eta = z/H$. The reduced windspeed is the ratio $u(\zeta,\eta)/u_0(\eta)$, and the windspeed reduction is $\epsilon = 1-u(\zeta,\eta)/u_0(\eta)$.

The windspeed reduction is considered a function of leeward distance and shelter density. The literature has contradicting results on how windspeed reduction depends on ζ and η. Some studies showed that windspeed reduction is greater in the near lee for denser shelters, and that the resulting shear produced more turbulence that allowed the flow to recover within a short distance compared to more porous shelters (Eimern et al., 1964). Other studies (Wilson, 1985; Heisler and DeWalle, 1988) seemed to indicate that denser (less porous) shelters provide more protection all the way to the point of full recovery. The argument was that the

turbulent eddies produced by the shelter are of small scale, are less efficient in transferring momentum and are thought to dissipate rapidly. Consequently according to Wilson (1985) the denser shelter provided more protection at all distances downwind. We used our numerical model to study this issue.

The model was set to run several times by incrementing the porosity parameter S at each time. The roughness height was set at z_0=0.01 m. The reduced windspeed at η=0.5, for S varying from 0.5 to 2.5 is depicted in Fig. 26. The model results show that for small values of S (up to 1.5), denser shelters provide more protection at all distances in the lee. The S=2 curve indicates more reduction in the near lee, but at ζ=5 and beyond the normalized windspeed becomes larger for S=2, than for S=1.5. It even asymptotically approached the one for S=1 around ζ=10. When the shelter density increased to S=2.5, the normalized windspeed remained smaller than that for less porous shelters. The same pattern is observed for η=1/3 (Fig. 27), and η=2/3 (Fig. 28).

These results indicate that for intermediate porosity there is more protection in the lee, but the flow recovers within a shorter distance in the lee. The model results, therefore, agree with the conclusions by Eimern et al. (1964). For low and high porosity, however, the simulations indicate more protection by denser shelters all the way, which supports the claim by Wilson (1985). Commenting on the experimental

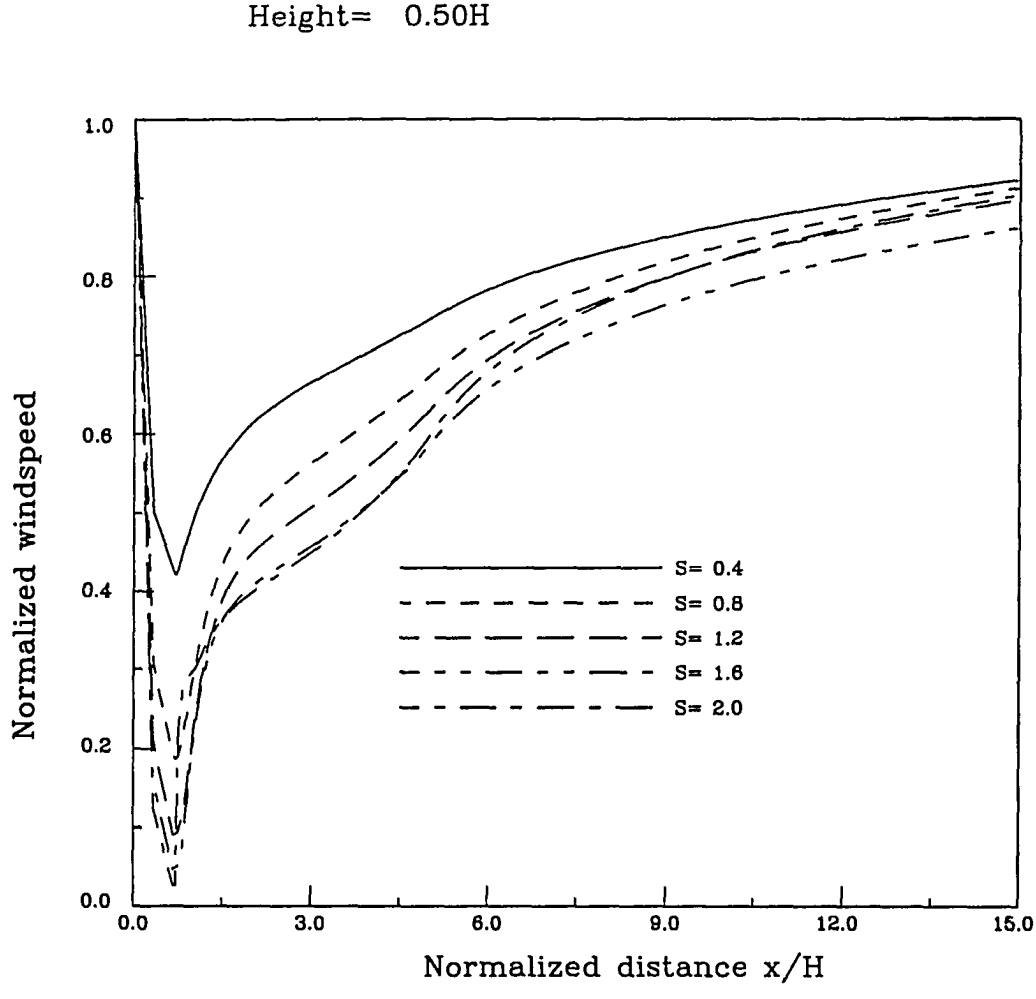

Fig. 26. Reduced windspeed for different shelter densities in the lee at z=H/2.

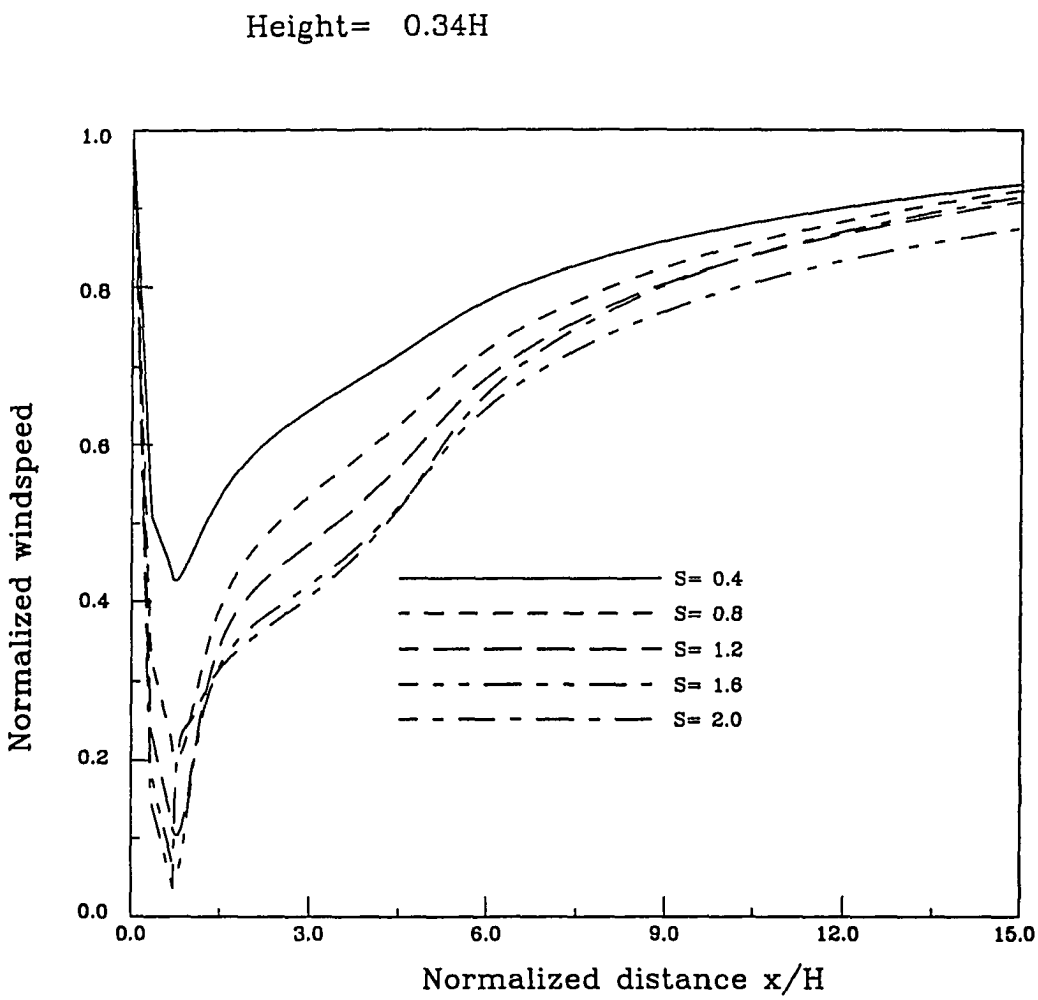

Fig. 27. Reduced windspeed for different shelter densities in the lee at z=H/3.

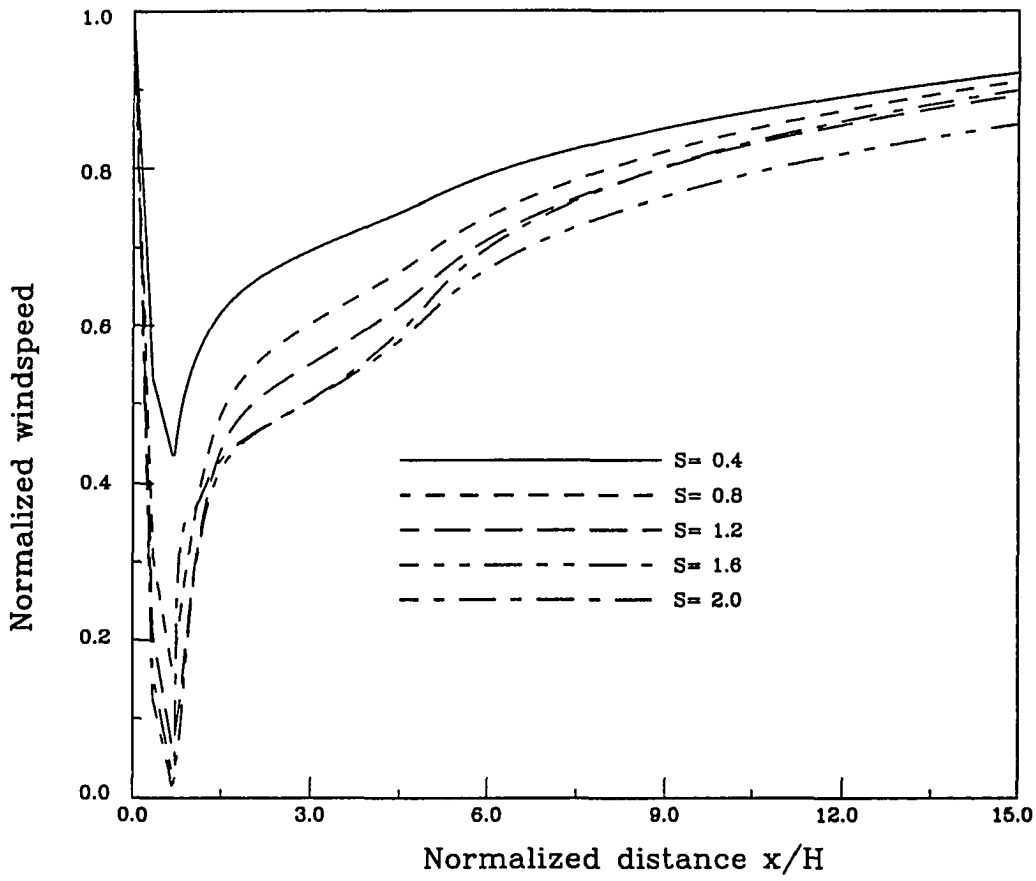

Fig. 28. Reduced windspeed for different shelter densities in the lee at z=2H/3.

findings on the effects of windbreak porosities on the rate of recovery toward the upstream equilibrium condition, Wilson (1985) stated that the data of Hagen and Skidmore (1971b), Hagen et al. (1981), and Raine and Stevenson (1977) unambiguously showed that the downwind extent of shelter protection increased as the porosity decreased. This was simply not true, because the data of Hagen and Skidmore did indicate that for η=0.5 and H/z_0=260, the recovery to 80% of the upstream equilibrium was at leeward distances of ζ=20, ζ=22, and ζ=19 for respective porosities of 60%, 40%, and 20%. Clearly the 40% porous windbreak protection extended beyond the 20% porous one.

Hagen et al. (1981) developed a model and compared the simulated results with data of Hagen and Skidmore (1971b) among others. In this case the simulations indicated that the recovery to 60% for a 60% porous shelter took place at ζ=4, while Wilson (1985) reported it at ζ=7.5. Although this misrepresentation did not affect the overall conclusion about the downstream extent of wind reduction as a function of porosity, we believe that credibility and importance should be attached to the observational data. Furthermore the observations of Naegeli (1946) reported in Eimern et al. (1964), when disregarding the very dense case, were in good agreement with the present study. When the density is high a recirculation bubble forms, and the numerical scheme and the

physics used in the present model were not designed to deal with the singularity that exists at the limit of the bubble.

Wilson (1985) had based his conclusion on numerical simulations, including his own, that in some cases disagreed with the observations (Hagen et al. 1981; Naegeli, 1946), and wind tunnel studies (Raine and Stevenson, 1977). The full scale experimental data and the present model simulations did not agree with his conclusions.

B. Shelter Efficiency

The simulation results were used to compute the shelter efficiency which is defined as:

$$\sigma=\int_0^{\zeta_1}\varepsilon(\zeta,\eta)\,d\zeta \tag{28}$$

Normally the upper limit of the integral should be infinity. But for practical reasons ζ_1 is set to be a distance where the flow recovers a large percentage of its upstream velocity (it is arbitrarily set at 15H here). The integration of ϵ is carried out using the composite Simpson's rule by which the integral of a function f(x), known at equally spaced points x_0, $x_{1/2}$, x_1, $x_{3/2}$, x_2, ..., x_N is evaluated as follows:

$$\int_{x_0}^{x_N} f(x)\,dx=\frac{h}{6}\left[f_0+f_N+2\sum_{i=1}^{N-1} f_i+4\sum_{i=1}^{N} f_{i-1/2}\right] \tag{29}$$

where $h=x_i - x_{i-1}$ (Conte and de Boor, 1980)

The shelter efficiency is computed at η=0.5 for three

different roughness heights, and for S varying from 0.4 to 2.2 with a 0.2 increment. The results are summarized in Table 9. Table 9 shows that σ decreases with increasing roughness height for all values of S that were tested. Efficiency increases up to a maximum value then decreases with increasing shelter density. This maximum value is not reached for the S values tested when the surface is smooth (z_0=0.01), and it appears to be reached at smaller values of S for rougher surfaces. This result is in good agreement with the wind tunnel observations by Jensen (1954) and our findings in the previous section about the existence of an optimum porosity that is neither too high nor too low. In order to look for an optimum S, one has to determine the upwind roughness height (see Appendix B for methods of estimating the roughness height from the surface elements height). The blanks on Table 9 are due to the appearance of reverse flow at high density.

C. Effects of Turbulence in the Approach Flow on Windspeed Reduction

The first clear demonstration in the field that an increase in approach flow turbulence caused poorer windspeed reduction downwind of shelterbelts and windbreaks, came from the results of Jensen (1954). Guyot (1986) made observations in the lee of a windbreak with and without induced turbulence

Table 9. Shelter efficiency as a function of z_0, and S.

S	z_0=0.01	z_0=0.05	z_0=0.10
0.4	22.02	19.76	18.33
0.6	25.84	23.40	21.79
0.8	28.04	25.54	23.82
1.0	29.61	27.16	25.49
1.2	31.25	28.48	26.58
1.4	34.01	31.25	27.08
1.6	34.61	31.35	25.95
1.8	35.56	33.02	24.54
2.0	36.41	32.57	-----
2.2	36.94	-----	-----

windward. The approaching flow was made turbulent by placing cylindrical horizontal bars. These bars were expected to induce turbulence in the flow without significantly affecting its velocity. It was observed that in the case of induced turbulence the windspeed reduction by the shelter was smaller. In other words shelters were less efficient in reducing windspeed when the approach flow was made more turbulent.

This phenomenon is very important to understand for it helps understand the effect of a shelterbelt network. Two simulations were run with two different TKE profiles: one of the profiles was the result from the first run at ζ=1.7 in the lee of a shelterbelt, and was larger than the upwind TKE profile used for the first run. These are illustrated by the

curves "ref. " in Fig. 29 and Fig. 30. The only source of turbulence is mechanical, and because the profile adjusts during the iteration, the difference in the vertical profiles of mean horizontal wind at the same distances is hardly noticeable (Fig. 31 and Fig. 32).

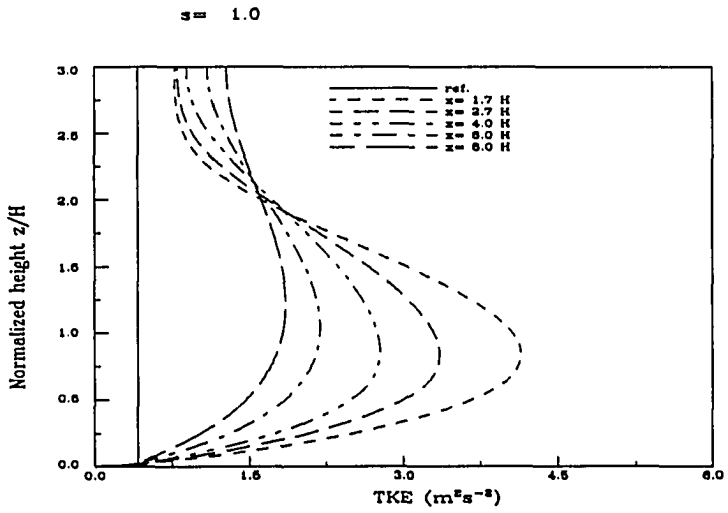

Fig. 29. TKE simulation results starting with a constant profile (denoted "ref").

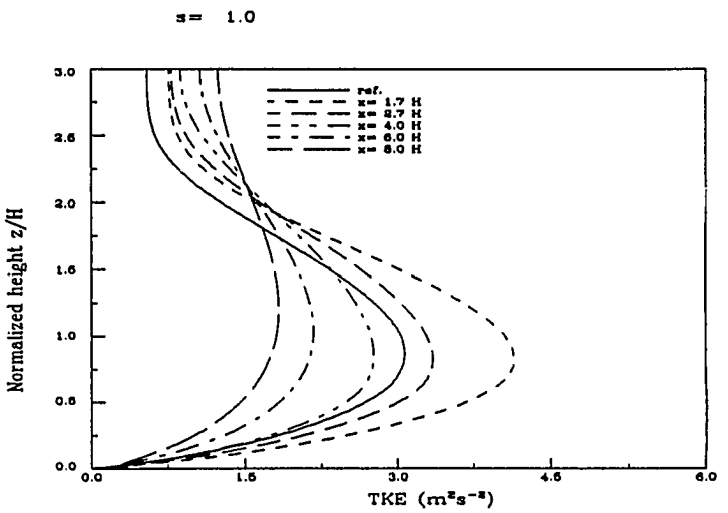

Fig. 30. TKE simulation results starting with a significant turbulence profile (denoted "ref.").

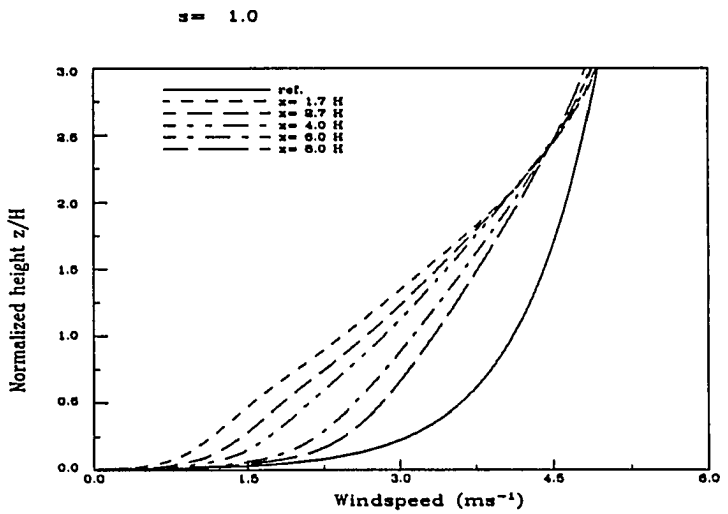

Fig. 31. Simulated profiles corresponding to Fig. 29.

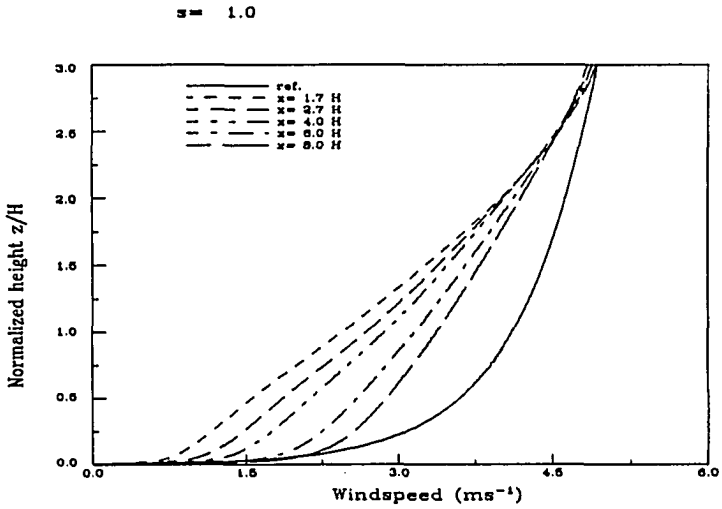

Fig. 32. Simulated profiles corresponding to Fig. 30.

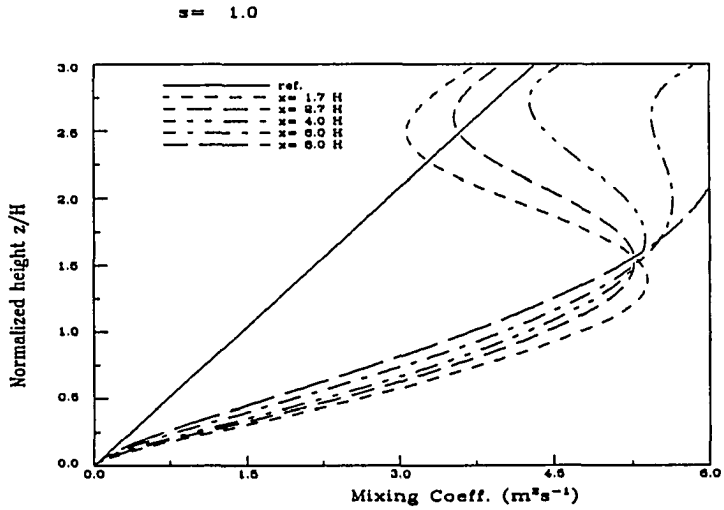

Fig. 33. Mixing coefficients corresponding to Fig. 29.

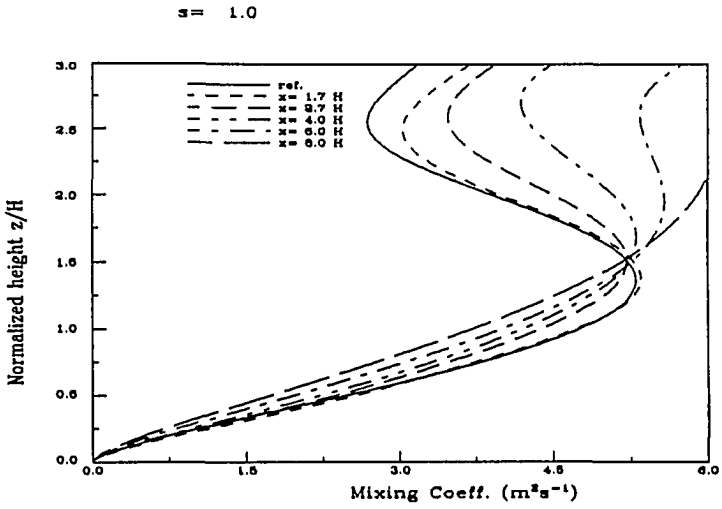

Fig. 34. Mixing coefficients corresponding to Fig. 30.

D. Shear Stress at the Surface

The shear stress exerted on the ground surface is determined by the vertical gradient of horizontal velocity. Since the speed is zero at the surface, higher ambient winds cause larger shear stress on the ground. The shear stress at the ground has serious implications in agriculture. Not only is it the main agent for soil wind erosion, but also it has tremendous effects drift of snow and sand.

By analogy of molecular diffusion in laminar flow to turbulent diffusion in the atmosphere, the shear stress τ is

expressed as $\tau=\rho K_m \frac{\partial u}{\partial z}$, and the velocity scale is taken to represent the wind shear stress at the ground $\tau_0=\rho u_*^2$. The normalized shear stress at the surface is given by $\frac{\tau}{\tau_0}=K_m \frac{\partial u/\partial z}{u_*^2}$. This quantity is computed from the simulations and plotted in Fig. 35.

The normalized shear stress, like the normalized windspeed, is smaller at all distances downwind for high porosities. But at S=2, there is more protection in the near lee which tends to recover to its upwind equilibrium a lot faster, such that around ζ=5, the protection with S=1.6 becomes better. This suggests that there is an optimum porosity for which the protected area could be largest and that is consistent with the behavior of the normalized windspeed. Around ζ=1, the shear stress is negative, which is an indication that the windspeed decreased with height.

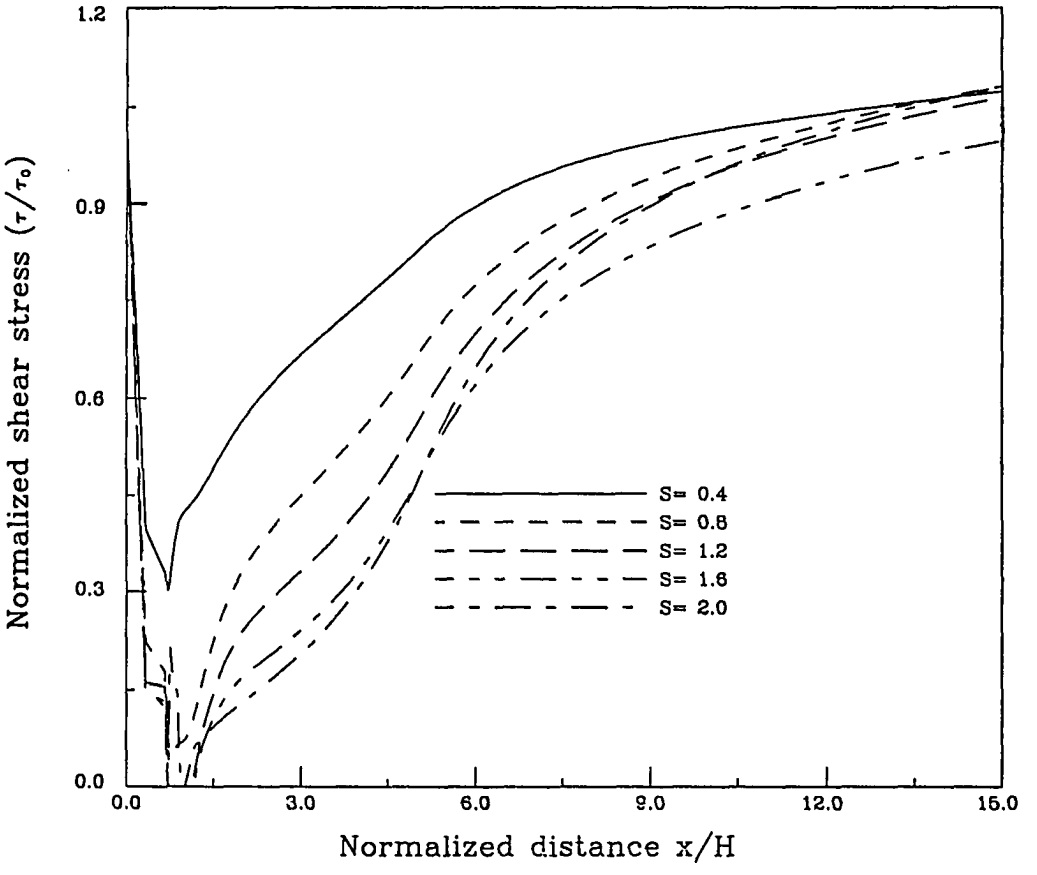

Fig. 35. Computed shear stress at the surface.

IV. TKE DISTRIBUTION IN THE LEE OF A SHELTERBELT

The study of turbulence patterns in the lee of porous barriers is extremely important for a better understanding of the sheltering effects. Not only is turbulence a result of interaction between the flow and the shelter immersed into it, but it also has a significant effect on the efficiency of a shelterbelt network. Turbulence was used to explain differences in windspeed reduction behind identical barriers. In the case of a network the first barrier plays the role of turbulence generator, and the ones downwind have a reduced efficiency as a result. TKE is directly related to the momentum, heat, and moisture transport in the boundary-layer. The individual terms in the TKE budget equation (Eq. 12) describe physical processes that generate or suppress turbulence. The relative importance of these processes determines the ability of the flow to maintain or suppress turbulence, or to become turbulent.

A. TKE Budget Terms

The TKE budgets at four downwind locations is plotted in Figs. 36-38. Individual terms are discussed below.

1. Advection

For flow over flat terrain it is often assumed that there is little horizontal and vertical variation in TKE within the

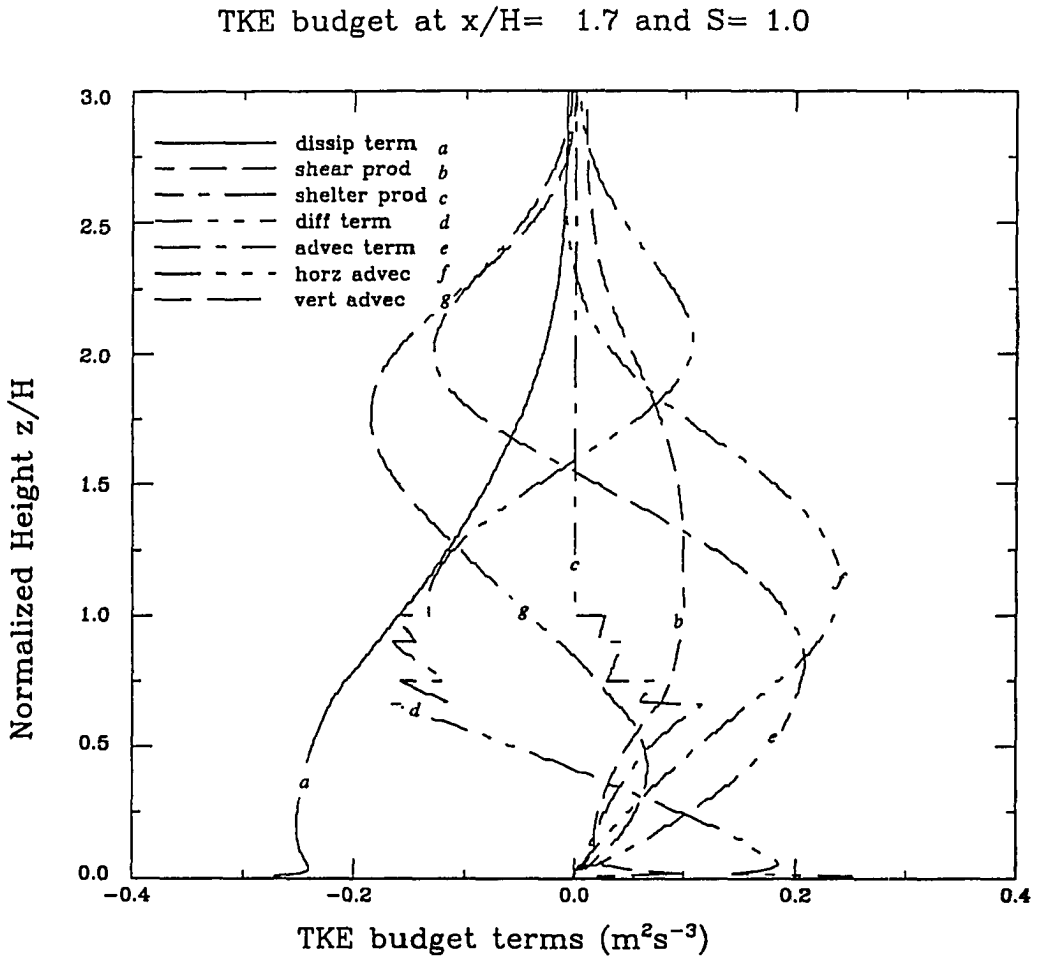

Fig. 36. Simulated budget terms at 1.7H in the lee of a porous shelterbelt.

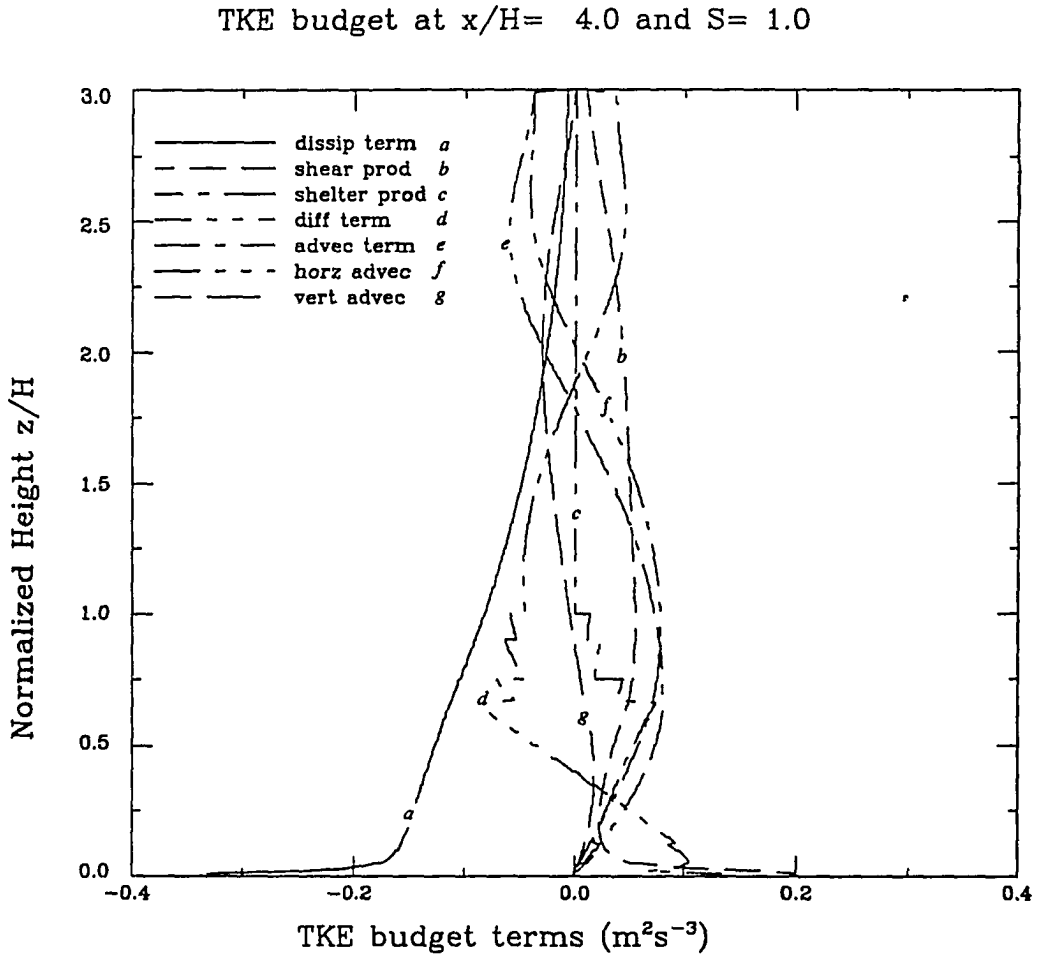

Fig. 37. Simulated budget terms at 4H in the lee of a porous shelterbelt.

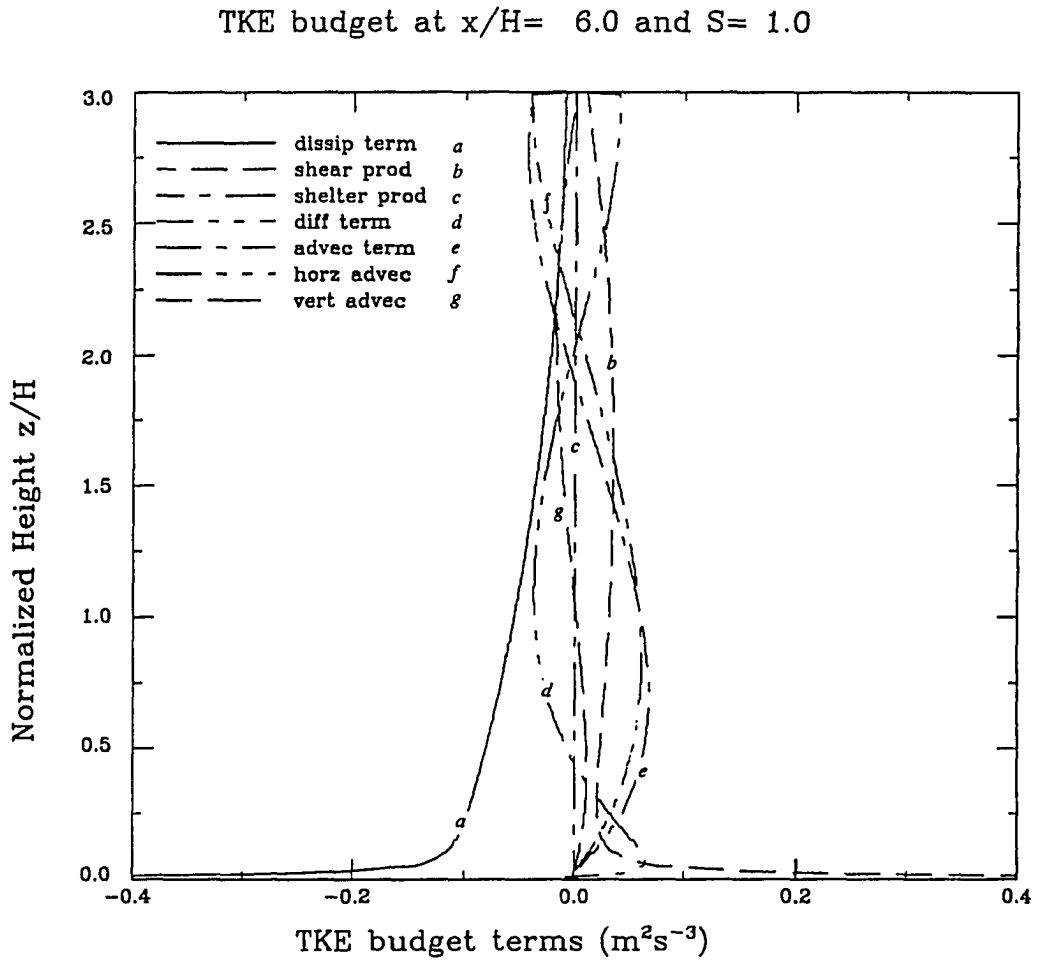

Fig. 38. Simulated budget terms at 6H in the lee of a porous shelterbelt.

surface layer, thereby making the advection term negligible. For shelterbelts and windbreaks, however, there is a tremendous production of TKE in their near lee and also close upwind with a maximum around η=1. The TKE is observed to increase by more than 50% of its upstream value up to η=2 (Finnigan and Bradley, 1983). A mean wind advecting air across a shelterbelt would thus cause a significant change in the TKE through advection.

The horizontal advection $-u\frac{\partial e}{\partial x}$ is a gain up to η=2.2 (Fig. 35), because below that level, the TKE decreases with increasing leeward distances. It has a peak at about η=1, which coincides with the level of maximum TKE production by the shelter. The TKE thus produced is then advected and diffused vertically. This creates a region above which the TKE increases with increasing leeward distances, resulting into a little loss of TKE by horizontal advection.

The vertical advection $-w\frac{\partial e}{\partial z}$ is a gain up to the maximum of TKE production at about η=1 (Fig. 36). It then becomes a loss above that level in the region where TKE decreases with height.

2. Shear production

The interaction between turbulent momentum flux and the mean wind shear generates more turbulence. In its

parameterized form the shear production is $K\left(\frac{\partial u}{\partial z}\right)^2$ and is always positive. It is largest at the bottom, gets smaller in the region of strong windspeed reduction where the profile becomes almost constant with height, picks up and has another maximum above the top of the shelter, and then decreases to a low value at the top of the domain (η=3).

3. Shelter production

This term is unique to flow crossing shelterbelts. When the flow crosses a porous shelter the drag forces oppose the flow and act as a momentum sink. The flow is forced to partially go above the shelter, and partially cross through the openings or pores. The ratio of the mass of air passing through to that forced above is determined by the porosity. This situation creates a turbulent wake in the lee. The turbulence thus generated is produced by the shelter. The shelter production term increases from the bottom to about η=0.7, then decreases like a step function, to become zero at the top of the shelterbelt (η=1).

4. Turbulent diffusion

Overall the turbulent diffusion term also known as turbulent transport or flux divergence term does not create nor does it destroy turbulence, but it just moves or redistributes turbulence from one level to another.

Nevertheless, it does act as TKE production or loss term locally, depending on whether there is flux convergence or divergence. The diffusion term is positive indicating a gain from the ground up to η=0.5 the first inflexion point in the TKE profile. This is the region where the TKE vertical gradient increases with height. Above that point the TKE vertical gradient starts decreasing and the turbulent diffusion term becomes a loss up to η=1.5. At first the gradient is positive up to the level of maximum TKE and then turns negative past the TKE maximum level, but continues decreasing up to η=1.5. This is another inflexion point in the TKE profile. Above that point the negative gradient values start increasing (that is, getting smaller in absolute values), and consequently the transport term again becomes a gain. This suggests that the TKE profile has two inflexion points of the curve; the TKE is diffused or transported by the eddies upward and downward from the region of maximum production (between the two inflexion points).

5. Dissipation term

The viscous dissipation term is the rate at which TKE is converted into internal energy by working against the viscous stresses. The destruction of turbulent motions is greatest for the smallest eddies and the small-scale turbulence is, in turn, driven by the cascade of energy from larger scales.

Thus the dissipation term is a loss term that is largest at the surface and decreases all the way up, as the eddies aloft are larger.

At subsequent locations downwind (Figs. 37-38), all terms get smaller and smaller as the distance from the shelter increases, because turbulence created in the near lee, between η=0.5 and η=1.5, is advected and diffused leeward and to higher levels. It is also cascaded to smaller-scale turbulence and dissipated at low levels. At ζ=6 all terms flatten out, but the dissipation and the shear production become very large below η=0.1.

B. TKE Profiles

The TKE profiles are very consistent with the budget term profiles. Below roughly η=2 the TKE decreases with increasing leeward distance. Since u is positive, $-u\frac{\partial e}{\partial x}$ is also positive but above η=2 the reverse is true. The TKE at any distance downwind has its peak near η=1, in good agreement with the profiles of Hagen et al. (1981). The energy is partly cascaded downward then dissipated, and partly transported upward as one moves further downwind. This also shows good agreement with the results of Hagen et al. (1981), and Finnigan and Bradley (1983).

V. CONCLUSIONS AND RECOMMENDATIONS

The data show that the wind direction for oblique flows is altered by the shelter in the near lee. The wind angle with the normal to the shelter is observed to decrease as the flow crosses the shelterbelt. The flow deflection, thus observed, is due to the observed strong pressure gradient across the shelter.

A significant linear relationship with a negative slope was found at low level (below 0.5H) between the angle of incidence and the reduced windspeed in the lee, which is due to an increase of the distance travelled by the flow to cross the shelter. The data also revealed a positive linear relationship between the windspeed in the open and the reduced windspeed in the lee. The windspeed in the open is known to indirectly affect the reduced windspeed in the lee by affecting the density of a shelter like the one used for this experiment. For both cases the higher windspeed of the undisturbed flow created larger pressure gradients between the windward and leeward sides of the shelterbelt. Larger pressure gradients are known to impose more deflection on the flow, which in turn increases the effective porosity. This is thought to be a cause for the scatter in both regressions.

The model-simulated wind profiles compared well with mean set profiles obtained from the observations for two of the sets, and compared even better for mean profiles obtained from

runs with windspeed at the top of the mast greater than or equal to 5 m s^{-1}. For the third set, however, model results and observations did not compare well. The reversal of the pressure gradient in the lee produces a minimum, which is well documented in the literature. Its location depends on the shelter density and that is not captured by the model. The period during which the set in question was recorded was also the period when the windspeed was steadily decreasing. This steady decrease of the undisturbed windspeed is thought to have shifted the minimum core leeward to be centered at or close to 2H. As a result the windspeed at 2H was smaller than the one at 1H for $0.2H \leq z \leq 0.6H$. Nevertheless in general the simulations and observations agreed well, and the agreement was even better with high winds.

The validated model was also used to run simulations with different by varying S. The windspeed reduction at selected heights was then used to compute shelter efficiency (integrations were performed by the Composite Simpson Rule). It was found that for low S values (0.5 to 1.5) the higher the shelter density the more effective the shelter is in reducing windspeed. The same could be said for S values greater than 2. For intermediate values, however, the denser shelter yielded more reduction in the near lee, which was offset by a rapid rate of recovery. This is in total agreement with the data by Nagaeli (1946) reported in Eimern et al. (1964), but

in disagreement with Wilson's (1985) conclusions about shelter efficiency.

The simulated TKE profiles were found to agree qualitatively well with previous work (Hagen et al., 1981, and Finnigan and Bradley, 1983). The shear stress at the ground was consistent with the simulated wind profiles, and in good agreement with observations by Bradley and Mulhearn (1983), as well.

The model simulates wind profiles more accurately for strong winds. The profiles thus simulated could be used for many purposes. Mean wind profiles are needed for the computation of evapotranspiration (Rosenberg et al. 1983), they could also be used to compute soil-eroding forces (Skidmore and Hagen, 1977). Other derived quantities such as shear stress and shelter efficiency are also useful in assessing shelter protection. The model has the capability of finding optimal shelter density, which could be used for optimal shelterbelt design.

The overall model performance was considered satisfactory on the basis of a quantitative comparison of model profiles of windspeed with observations in the lee of a shelter; it could, therefore, used with confidence to simulate the flow in the near lee of a shelterbelt of similar structure to the one used in this study. Otherwise another tuning will be needed when the model is used for shelterbelt of different height and

width. Also, lack of field observations precluded comparisons of turbulence calculations with measurements.

The model performed well in simulating wind, but we have to bear in mind that the shelter density parameter was used as an adjusting device to account for the effects of both incidence angle and windspeed. If S is actually measured, this adjustment will not be possible. Thus studying the effect of angle of incidence on model performance with S measured will allow for improvement of model capability for diagnosing shelterbelt aerodynamics and evaluation of limitations for applications to oblique winds.

The above conclusions were drawn from one measurement set that might not be representative of all cases. Thus, longer sets of repeated series of measurements are needed, for repeated measurements reduce the variation among experiments and lead to more reliable conclusions.

REFERENCES

Ajayi, F., S. Anza, S. Horst, P. Pradervan, and B. Ephson. 1990: Holding back the desert. *African Farmer: The Key to Africa's Future*. **3:** 17-21

Bean, A., and R. W. Alperi, and C. A. Federer. 1975: A method for categorizing shelterbelt porosity. *Agric. Meteorol*. **14:** 417-429.

Bilbro, J. D., and D. W. Fryrear. 1988: Annual herbaceous wind barriers for protecting crops and soils and managing snowfall. *Agric. Ecosyst. and Environ*. **22/23:** 149-161.

Borrelli, J., J. M. Gregory, and W. Abtew. 1989: Wind Barriers: a revaluation of height, spacing and porosity. *Trans. ASAE* **32:** 2023-2027.

Bradley, E. F., and P. J. Mulhearn. 1983: Development of velocity and shear stress distributions in the wake of a porous shelter fence. *J. Wind Eng. Ind. Aerodyn*. **15:** 145-156.

Brandle, J. R., B. J. Bruce, and T. Akeson. 1992: Field windbreaks: Are they economical? *J. Prod. Agric*. **5:** 393-398.

Caborn, J. M. 1957: Shelterbelts and microclimate. *For. Comm. Bull*. No 29, Edinburgh, p 129.

Conte, S. D., and C. de Boor. 1980: Elementary numerical analysis: An algorithmic approach. Third edition. McGraw-Hill, New York. p 432.

Counihan, J., J. C. R. Hunt, and P. S. Jackson. 1974: Wakes behind two-dimensional surface obstacles in turbulent boundary-layers. *J. Fluid Mech.* **64:** 529-563.

Denuyl, D. 1936: The zone of effective windbreak influence. *J. Forest.* 689-695.

Eimern, J. V., R. Carschon, L. A. Razumova, and G. W. Robertson. 1964: Windbreaks and shelterbelts. *World Meteorol. Org. Tech. Note No 59.*

Finnigan, J. J., and E. F. Bradley. 1983: The turbulent kinetic energy budget behind a porous barrier: an analysis in stream-line coordinates. *J. Wind Eng. Ind. Aerodyn.* **15:** 157-168.

Grace, J. 1988: Plant response to wind. *Agric. Ecosyst. and Environ.* **22/23:**71-88.

Guyot G. 1986: Brise-vent et rideaux abris avec référence particulière aux zones sèches. Cahier F.A.O. 15, Rome, p 385.

Guyot, G., and B. Séguin. 1978. Influence du bocage sur le climat d'une petite région: Résultats des mesures éffectuées en Bretagne. *Agric. Meteorol.* **19:** 411-430.

Hagen, L. J., and E. L. Skidmore. 1971a: Windbreak drag as influenced by porosity. *Trans. ASAE* 464-465.

Hagen, L. J., and E. L. Skidmore. 1971b: Turbulent velocity fluctuations and vertical flow as affected by windbreak porosity. *Trans. ASAE* 634-637.

Hagen, L. J., E. L. Skidmore, P. L. Miller, and J. E. Kipp. 1981: Simulations of effects of wind barriers on air flow. *Trans. ASAE.* 1002-1008.

Heisler, G. M., and D. R. DeWalle. 1988: Effects of windbreak structure on wind flow. *Agric. Ecosys. Env.* **22/23:** 41-69

Jensen, M. 1954: Shelter Effect: investigation into the aerodynamics of shelter and its effects on climate and crops. *The Danish Technical Press.* Copenhagen. p 264.

Kaimal, J. C., and J. J. Finnigan. 1994: Atmospheric boundary layer flows: their structure and measurement. *Oxford University Press.* Oxford. p 289.

Kort, J. 1988: Benefits of windbreaks to field and forage crops. *Agric. Ecosys. Env.* **22/23:** 165-190.

Litvina, I. V. 1987: Meteorological recommendations for designing and using plant corridors. Agrophysical Institute Saint-Petersburg, Russia. p 41.

Litvina, I. V, and E. S. Takle. 1992: Development, testing, and application a turbulence model for a shelterbelt design. Unpublished manuscript. p 11.

Lyles, L. 1988: Basic wind erosion processes. *Agric. Ecosys. Env.* **22/23:** 91-101.

Maki, T. 1982: Studies on windbreak nets: Micro-meteorological modification of a cool weather damage of

paddy rice and turbulent characteristics influenced by windbreak nets. *Bull. Natl. Inst. Agric. Sci. Ser.* **A29:** 1-45.

Maki, T., and L. H. Allen. 1978: Turbulence characteristics of a single line pine tree windbreak. *Proc. Soil Crop Sci Florida.* **37:** 82-92.

McNaughton, K. G. 1988: Effects of windbreaks on turbulent transport and microclimate. *Agric. Ecosyst. Environ.* **22/23:** 17-39.

Miller, D. R., N. J. Rosenberg, and W. T. Bagley. 1975: Wind reduction by a highly permeable tree shelterbelt. *Agric. Meteorol.* **14:** 321-333.

Mulhearn, P. J., and E. F. Bradley. 1977. Secondary flows in the lee of porous shelterbelts. *Boundary-Layer Meteorol.* **12:** 75-92.

Naegeli, W. 1946: Weitere untersuchungen über die windverhältnisse im bereich von windschutzanlagen. *Mitt. Schweiz Anst. Forstl. Versuchswesen* **24:** 660-737.

Ogawa, Y., and P. G. Diosey. 1980: Surface roughness and thermal stratification effects on the flow behind a two-dimensional fence: I. Field study. *Atmos. Environ.* **14:** 1301-1308.

Oreskes, N. K., S. Frechette, and K. Belitz. 1994. Verification, validation and confirmation of numerical models in the earth sciences. *Sci.* **263:** 641-646.

Panfilov, J. D. 1948: Forest shelterbelt. Oblgiz, Saratov.

Panofsky, H. A., and J. A. Dutton. 1984. Atmospheric Turbulence. John Wiley & Sons, Inc. New York. p 397.

Patankar, S. V. 1980: Numerical heat transfer and fluid flow. Hemisphere Publishing Corp., London. p 197.

Pedlosky, J. 1987: Geophysical fluid Dynamics. Second Edition Springer-Verlag, New York. p710.

Perera, M. D. A. E. S. 1981: Shelter behind two-dimensional porous and solid fences. *J. Wind Eng. Ind. Aerodyn.* **8:** 93-104.

Plate, E. J. 1971: Aerodynamics of shelterbelts. *Agric. Meteorol.* **8:**203-222

Radke, J. K. 1976: The use of annual wind barriers for protecting row crops. In: R. W. Tinus (editor), *Proc. Symp. Shelterbelts on the Great Plains.* 20-22 April, Denver, CO, USA. Great Plains Agric. Council Pub. No 78: 79-86.

Raine, J. K., and D. C. Stevenson. 1977: Wind protection by model fences in a simulated atmospheric boundary-layer. *J. Ind. Aerodyn.* **2:** 159-180.

Rider, N. E. 1952: The effect of a hedge on the flow of air. *J. Meteorol. Soc. Quart. Rept.* **78:** 97-101.

Ronneberg, E. 1992: The hedgerow project. The Hedgerow Foundation, Chicago, Illinois. p 40.

Schmidt, R. A., and R. L. Jairell. 1993: Shelterbelt wind profile measurement: Database documentation -- September 1993. Unpublished manuscript. p 11.

Schmidt, R. A., and R. L. Jairell. 1994: Shelterbelt wind profile measurement: Database documentation -- May 1994. Unpublished manuscript. p 8.

Scholten, H. 1988: Snow distribution on crop fields. *Agric. Ecosys. Env.* **22/23:** 363-380.

Seginer, I. 1972: Windbreak drag calculated from the horizontal velocity field. *Boundary-Layer Meteorol.* **3:**87-97

Seginer, I., and R. Sagi. 1972: Drag on windbreak in a two-dimensional flow. *Agric. Meteorol.* **9:** 323-333.

Seginer, I. 1975a: Atmospheric stability effect on windbreak shelter and drag. *J. Boundary-Layer Meteorol.* **8:** 383-400.

Seginer, I. 1975b. Flow around a windbreak in oblique wind. *Boundary-Layer Meteorol.* **9:** 133-141.

Sheih, C. M., P. J. Mulhearn, E. F. Bradley, and J. J. Finnigan. 1978: Pollutant transfer across the cavity region behind a two-dimensional fence. *Atmos. Env.* **12:** 2301-2307.

Skidmore, E. L., and L. J. Hagen. 1977: Reducing wind erosion with barriers. *Trans. ASAE* 911-915.

Stull, R. B. 1988: An introduction to boundary layer meteorology. Kluwer Academic Publishers. Boston. p 666.

Sturrock, J. W. 1969: Aerodynamic studies of shelterbelts in New Zealand-1. *New Zealand J. Sc.* **12:** 754-776.

Sturrock, J. W. 1972: Aerodynamic studies of shelterbelts in New Zealand-2. *New Zealand J. Sc.* **15:** 113-140.

Takahashi, H. 1978: Wind tunnel test on the effect of windbreaks on the wind speed distribution leeward. *J. Agr. Meteorol.* **33** (4): 183-187.

Wilson, J. D. 1985: Numerical studies of flow through a windbreak. *J. Wind Eng. Ind. Aerodyn.* **21:** 119-154.

Wilson, J. D. 1987: On the choice of a windbreak porosity profile. *J. Boundary-Layer Meteorol.* **38:** 37-49.

Woodruff, N. P., and A. W. Zing. 1955: A comparative analysis of wind-tunnel and atmospheric air-flow patterns about single and successive barriers. *Trans. Am. Geophys. Union* **36:** 203-212.

ACKNOWLEDGEMENTS

I would like to take this opportunity to express my thanks and gratitude to those individuals and agencies who have assisted me toward the completion of my graduate program.

First, I would like to thank my advisor Eugene S. Takle for his support and patience. I would also like to extend my thanks to my dissertation committee Dr. R. Carlson, Dr. P. Hinz, Dr. R. Horton, and Dr. E. Taylor.

My thanks also go to Iowa State employees Dr. R. Turner for having provided a basic NCAR GRAPHICS code, G. Underwood for having helped whenever a computer related problem arose, and Z. Ötles who, despite his busy schedule, has often taken some time to help me with McCintosh plotting software.

I would like to thank Dr. Irina V. Litvina of the Agrophysical Institute (St Petersburg, Russia) for having provided the basic part of the shelterbelt numerical model code.

My thanks also go to my fellow graduate students Creig Clark, Weidong Jiang, Zaitao Pan, Paul Thomson, Dennis Todey, Christopher Wikle, who have made the third floor a nice working environment.

Without the financial support of the African American Institute and the Iowa State University Agriculture and Home Economics Experiment Station, the completion of my graduate program would not have been possible. I would like to say

thanks.

Finally I would like to thank my wife Zahra, my twin boys Mehawesh and Kabbod for their patience, and my family and friends back home, especially my childhood buddy Hamid Abdel Kerim, for their support and encouragements.

APPENDIX A:

FURTHER DETAIL OF THE EQUATIONS TREATMENT

A. Intermediate Steps in the Momentum and TKE Equations

The way the momentum and the TKE equations are treated here is unique to this model and deserves some attention. Ordinarily the boundary-layer equations are solved for the velocity components as they appear in the equations of motion. Here, for the sake of numerical instability control, it is considered that there exists a basic flow upon which a shelter-induced perturbation is superimposed. Under neutral conditions the basic flow velocity u_0 profile follows the logarithmic law. It is assumed to be known provided that the friction velocity and the roughness height are known:

$$u_0=\frac{u_*}{k}\ln\left(\frac{z+z_0}{z_0}\right) \qquad \text{(A1)}$$

The TKE of the undisturbed flow is taken as $e_0 = C_1^{-1/2}u_*^2$. The solution is sought for the shelter induced perturbations u_1 (for the wind velocity) and e_1 (for the TKE) such that $u=u_0 + u_1$ and $e=e_0 + e_1$ where u and e are, respectively, the actual velocity and TKE in the lee of a shelterbelt. The vertical velocity in the open is taken to be zero.

When u is substituted by $u_0 + u_1$ in Eq. 11, we get the following equation:

$$u\frac{\partial u_1}{\partial x}+w\frac{\partial u_1}{\partial z}=\frac{\partial}{\partial z}\left(K\frac{\partial u_1}{\partial z}\right)-\frac{u_*}{k(z+z_0)}\left(w+\frac{K}{z+z_0}-\frac{\partial K}{\partial z}\right)\Bigg\} \\ -C_f S u_0\frac{(u^2+w^2)^{1/2}}{2}-C_f S u_1\frac{(u^2+w^2)^{1/2}}{2}\Bigg\} \tag{A2}$$

When the same type of substitution is done for e Eq. 12 becomes

$$u\frac{\partial e_1}{\partial x}+w\frac{\partial e_1}{\partial z}=\frac{\partial}{\partial z}\left(\alpha_e K\frac{\partial e_1}{\partial z}\right)+K\left(\frac{u_*}{k(z+z_0)}+\frac{\partial u_1}{\partial z}\right)^2-\frac{u_*^4}{K}\Bigg\} \\ +C_f S u^2\frac{(u^2+w^2)^{1/2}}{2}-\left(\frac{C_1}{K}e_1+2\frac{C_1^{1/2}u_*^2}{K}\right)e_1\Bigg\} \tag{A3}$$

The forms of Eqs. A2 and A3 correspond to Eq. 14. These equations are linearized by first lagging the coefficients, then simply updating them after each iteration until convergence is achieved.

The solution of u is then used in the continuity equation to solve for the vertical velocity w according to the following discretized form:

$$\frac{1}{\Delta x}(u_{i+1,j}-u_{i,j})+\frac{1}{2\Delta z}(w_{i+1,j+1}-w_{i+1,j-1})=0 \tag{A4}$$

B. The Modified Tridiagonal Algorithm

Eq. 25 gives a simple relationship that uses the top and bottom boundary conditions to compute the coefficients from known quantities and then solve for the unknown. Eq. 19 for

j=1 gives $\alpha_1 f_0 + \beta_1 f_1 + \gamma_1 f_2 = \delta_1$ where f_0 is known. From this relationship we get

$$f_1 = -\frac{\gamma_1}{\beta_1} f_2 + \frac{\delta_1 - \alpha_1 f_0}{\beta_1} \quad \text{or} \quad f_1 = A_1 f_2 + B_1 \tag{A5}$$

For j=2 Eq. 19 yields $\alpha_2 f_1 + \beta_2 f_2 + \gamma_2 f_3 = \delta_2$. Considering Eq. A5

it follows that

$$\alpha_2 (A_1 f_2 + B_1) + \beta_2 f_2 + \gamma_2 f_3 = \delta_2 \tag{A6}$$

After some algebraic manipulations we get

$$f_2 = -\frac{\gamma_2}{\beta_2 + \alpha_2 A_1} f_3 + \frac{\delta_2 - \alpha_2 B_1}{\beta_2 + \alpha_2 A_1} \tag{A7}$$

The relationship is correct for j=2. We assume that it is correct for j=n-1, which implies that $f_{n-1} = A_{n-1} f_n + B_{n-1}$, and we'll try to prove that it is correct for j=n:

$$\alpha_n f_{n-1} + \beta_n f_n + \gamma_n f_{n+1} = \delta_n \tag{A8}$$

Substituting for f_{n-1}, we get

$$\alpha_n (A_{n-1} f_n + \beta_{n-1}) + \beta_n f_n + \gamma_n f_{n+1} = \delta_n \tag{A9}$$

This leads to

$$f_n = -\frac{\gamma_n f_{n+1}}{\alpha_n A_{n-1} + \beta_n} + \frac{\delta_n - \alpha_n B_{n-1}}{\alpha_n A_{n-1} + \beta_n} \tag{A10}$$

By analogy to Eq. 25 $A_n = -\frac{\gamma_n}{\alpha_n A_{n-1} + \beta_n}$ $B_n = \frac{\delta_n - \alpha_n B_{n-1}}{\alpha_n A_{n-1} + \beta_n}$. This completes the proof by induction.

C. Discretization of K

The length scale is $l=K/\sqrt{e}$, substituting this value in Eq. 26 gives:

$$\left.\begin{aligned} kC_1^{1/4}\frac{\sqrt{e}}{K} &= -\frac{K}{e}\frac{\partial}{\partial z}\left(\frac{e}{K}\right)+kC_1^{1/4}\frac{S}{A} \\ &= -\frac{K\frac{\partial e}{\partial z}-e\frac{\partial K}{\partial z}}{eK^2}+kC_1^{1/4}\frac{S}{A} \end{aligned}\right\} \tag{A11}$$

After some algebraic manipulations we get the following equation

$$\frac{\partial K}{\partial z}=\frac{K}{e}\frac{\partial e}{\partial z}+kC_1^{1/4}(\sqrt{e}-KS/A) \tag{A12}$$

Eq. 12 is discretized such that ΔK_m is computed from

$$\Delta K=kC_1^{1/4}(\sqrt{e}-K_jS/A)\Delta z+\frac{K_j}{e_{i,j}}(e_{i,j+1}-e_{i,j}) \tag{A13}$$

Finally K(j+1) = K(j) + ΔK (A14)

APPENDIX B:
ROUGHNESS HEIGHT AND FRICTION VELOCITY

Frictional drag causes the mean windspeed to become zero at the surface while the pressure gradient forces cause the wind to increase with height. Under neutral conditions the wind profile in the surface-layer is logarithmic. The surface stress, represented by the friction velocity u_*, and the surface roughness, represented by the roughness height, are key variables in the estimation of the logarithmic profile. The roughness height could be determined from measurement of the surface elements. It is also possible to determine both the roughness height and the friction velocity from wind profile measurements.

A. Direct Measurement of Roughness Height

The roughness height is not equal to the height of the individual roughness elements on the ground, but it does depend solely on the surface roughness. In other words it is not sensitive to changes in windspeed, stability or stress, but it does change only when the surface elements change.

When the surface roughness elements are evenly spaced, not too close together, and of similar height and shape, the estimation of the roughness height is based on the average vertical extent of the elements h, the average vertical cross-section area presented to the wind A_a and the lot size per element A_L (Stull, 1988).

$$z_0 = 0.5h\frac{A_a}{A_L} \tag{B1}$$

A_L=total ground surface area/number of elements.

When the element population is not uniform, differences among elements ought to be accounted for, in which case the roughness height is estimated by:

$$z_0 = \frac{0.25}{A_T}\sum_{i=1}^{N} h_i A_i \tag{B2}$$

where A_i is the horizontal surface occupied by element i, h_i its height, and A_T is the total area occupied by the N elements.

An approximation of the roughness height can also be obtained by summing over individual roughness elements encountered along a straight line of total length L_T. In this case the longitudinal width w_i of each element in the line is considered in place of s_i, so that

$$z_0 = \frac{0.25}{L_T}\sum_{i=1}^{N} h_i w_i \tag{B3}$$

B. Determination of Roughness Height and Friction Velocity from Observed Profile

It is also possible to get z_0 and u_* from the upwind observed profile of the velocity when measurements are available. By taking the ratio $\frac{u_i}{u_j}=\ln\left(\frac{z_i+z_0}{z_0}\right)/\ln\left(\frac{z_j+z_0}{z_0}\right)$ $(i\neq j)$, we just have one unknown in a non-linear equation that we could solve numerically by using the fixed point-iteration method. The equation will be of the following form:

$$g(z_0)=z_0=z_i/(((z_j+z_0)/z_0)^{u_i/u_j}-1) \qquad \text{(B4)}$$

This method will always converge provided that u_i and u_j fit in the same logarithmic profile since $|g'(z_0)|<1$ for $0<z_0<\infty$. If the method converges, then the velocity profile is logarithmic or nearly logarithmic. The friction velocity could, therefore, deduced from the velocity profile as well by using

$$u_*=ku/\ln((z+z_0)/z_0) \qquad \text{(B6)}$$

where k is the von Karman constant. In order for these parameters to better characterize the measured profiles, all 2x2 combinations of the measurement points are considered for the ratios u_i/u_j $(i\neq j)$ used in the computation of z_0. A first guess is provided for the ratio u_1/u_2. After convergence the result is added to the sum (sum=sum + $z_0(i,j)$), and $z_0(i,j)$ is used as a first guess for the next ratio. If convergence is

achieved for all N=n(n-1)/2 combinations (where n is the number of measurement points), then a mean $\overline{z_0}$ is computed by $\overline{z_0}=\sum_{i=1}^{N} z_{0i}/N$ and $u_*=\frac{k}{n}\sum_{i=1}^{n} u_i/\ln((z_i+z_0)/z_0)$. In case convergence cannot be achieved for up to 30% of the points, they will be considered as outliers and taken out. Only the remaining 70% of the points will be used to compute z_0 and u_*. If, however, the number of points where convergence can't be achieved is more than 30%, we could conclude that the upwind velocity profile is not logarithmic. It therefore cannot be used to compute z_0 and u_*. The user is given the choice to either start over with a different measurement profile, or to proceed with the run by entering a roughness height and a friction velocity.